DEVELOPMENT AND APPLICATION OF A NEW VOLTAGE STABILITY INDEX FOR ON-LINE MONITORING AND SHEDDING

By

Mariana Magdy Mounir Kamel

Ahmed H. Eltom
Professor of Electrical Engineering
Committee Chair

Abdelrahman A. Karrar
Visiting Professor of Electrical Engineering
Committee Co-Chair

Gary L. Kobet
Adjunct Professor of Electrical Engineering
Committee Member

DEVELOPMENT AND APPLICATION OF A NEW VOLTAGE STABILITY

INDEX FOR ON-LINE MONITORING AND SHEDDING

By

Mariana Magdy Mounir Kamel

A Thesis Submitted to the Faculty of the University of
Tennessee at Chattanooga in Partial Fulfillment
of the Requirements of the Degree of
Master of Science: Engineering

The University of Tennessee at Chattanooga
Chattanooga, Tennessee

August, 2016

ABSTRACT

During the past decades, voltage instability was the reason behind several major blackouts worldwide. Continuous assessment of the system voltage stability is vital to ensure a secured operation of the system. Several voltage stability indicators have been proposed and used in an attempt to quantify proximity to voltage collapse. Some of these are computationally expensive, and others are reported not to perform as expected under all conditions. In this work a new voltage stability indicator named the P-index is proposed. This index is based on normalized voltage and power sensitivities and as such, it provides an absolute measure of the system stability. It is robust and based on solid theoretical foundations. The index has been tested on static and dynamic test platforms, and for both platforms offered a correct assessment of proximity to voltage collapse and weakest system buses. Furthermore, a method for topology change detection suitable for online systems was proposed. Dynamic stability monitoring with PMU measurements was simulated in real-time on the well-known Kundur 10-bus system and the appropriate load shedding using the P-index was calculated. Compared to the another node-based indicator, the L-index, the results show that the P-index gives a better prediction of proximity to voltage collapse and is well suited for load shedding purposes.

DEDICATION

To Mariam … my angel in heaven

ACKNOWLEDGEMENTS

I would like to express the deepest appreciation to my professor Ahmed Eltom for believing in me and giving me the opportunity to be part of the research team at the University of Tennessee at Chattanooga.

I would also like to express my sincere gratitude to my supervisor Dr. Abdelrahman Karrar for his care, patience, encouragement, and immense knowledge. I consider myself to be extremely lucky to have a supervisor who cared so much for the completion and success of this project. Also I would like to thank my committee member Gary Kobet for his time and feedback on this project.

I would like to gratefully acknowledge the contribution of my friends Haytham Saeed, Elamin Mohamed and Mosab Zeyada to this work. I would also like to thank all my friends who experienced the ups and downs of my research. Thank you for always being there for me.

Last but not the least; I would like to express my deepest gratitude to my family. This journey would not have been possible if not for their unconditional love and support.

TABLE OF CONTENTS

LIST OF TABLES

LIST OF FIGURES

CHAPTER 1

INTRODUCTION

1.1 Overview

Voltage stability and voltage collapse have been a highly active research topic for decades. Even though voltage collapse has a low probability of occurrence, it certainly has a very high impact. Several major blackouts were reported to have been caused by voltage collapse. In general, voltage instability problems would normally occur in heavily loaded systems where a small disturbance such as a line outage may result in a situation where the system is no longer able to meet the reactive power demand. Early detection of voltage instability is necessary to prevent the system from collapsing. However, predicting voltage collapse proves to be a challenge.

1.2 Problem Statement

Several voltage stability assessment methods have been proposed in the literature. They all aim at quantifying proximity to collapse. However, a number of limitations have been reported in regard to these methods. Some exhibit nonlinear behavior due to discontinuities caused by system controls. Others are computationally expensive which makes them unsuitable for on-line applications. Some are found to be unreliable and work only in special cases. Some have even been proved to have unsound theoretical background. It is quite evident that there is still a need of a simple yet reliable voltage stability assessment tool.

1.3 Objectives

The first objective of this work is to develop a voltage stability indicator suitable for on-line assessment of the system voltage stability. This indicator is to quantify proximity to voltage collapse and pinpoint the weak bus or buses where load shedding would be most effective.

The second objective is to develop a load shedding scheme where the amount of load to be shed is sufficient for successful mitigation of voltage collapse and restoring the system to a stable operating state.

1.4 Thesis Layout

The remainder of this thesis is organized as follows:

- Chapter Two: this chapter provides an overview of the literature on voltage stability analysis methods: concepts and limitations.
- Chapter Three: this chapter introduces the concept behind the proposed voltage stability index along with the derivation of its formula and application to example systems. This chapter also presents the theory on how this index can be used to: a) estimate the margin of stability, b) determine, if necessary, the amount of load to shed.
- Chapter Four: this chapter presents simulation results and a discussion on the performance of the proposed index and load shedding method.
- Chapter Five: this chapter concludes the findings and contributions of this work. It also provides some suggestions and recommendations for further research work.

CHAPTER 2

LITREATURE REVIEW

2.1 Voltage Stability

According to IEEE/CIGRE joint task force on stability terms and definitions, voltage stability refers to *"the ability of a power system to maintain steady voltages at all buses in the system after being subjected to a disturbance from a given initial operating condition*" [1]. The three major factors contributing to voltage instability are: load dynamics, generation and transmission system limitations:

- Load dynamics: Voltage instability occurs when the load dynamics attempt to restore power consumption beyond the capability of the transmission network and the connected generation. When the voltage starts to drop after a disturbance, constant power loads such as industrial motor loads, air conditioners … etc tend to maintain their active power consumption through the action of motor slip adjustment, distribution voltage regulators, thermostats … etc. This would result in increasing the reactive power consumption which would cause the voltage to drop much further. In addition to the inherent dynamics of the load, on-load tap changers can have a major impact on the voltage stability of the system. In a highly stressed power system, it has been observed that raising the turns ratio in order to control the load bus voltage results in a decrease of voltage at that bus. This de-stabilizing effect is called reverse action of on-load tap-changer and is one of the mechanisms responsible for voltage collapse of power systems.

- Generation limits: If a disturbance occurs and as a result some of the generators hit their field or armature current time-overload capability limits, there will not be enough reactive power to support the system voltage.
- Transmission system limits: The third factor contributing to voltage instability is the voltage drop across the highly inductive transmission lines. This voltage drop limits the power transfer capability and voltage support of the transmission line. The power transfer and voltage support are further limited when the load on transmission lines is too high and/or the generation is too far from the load centers.

2.2 Voltage Collapse

According to IEEE/CIGRE joint task force on stability terms and definitions, voltage collapse is defined as "*the process by which the sequence of events accompanying voltage instability leads to a blackout or unacceptable low voltage profile in a significant part of the power system*" [1]. In other words, voltage collapse is a result of voltage instability. Voltage instability and voltage collapse have been responsible for several major blackouts throughout the world: New York 1970, France 1978 and 1987, Northern Belgium 1982, Tokyo 1987 … etc. The frequency and severity of these collapses has prompted significant research effort on the area of voltage instability and voltage collapse. Several static and dynamic analysis techniques have been proposed in the literature to examine proximity to voltage instability. Many authors have proposed what's known as voltage stability indices which aim at quantifying how 'close' the system is to the point of voltage collapse. Some of these indices are intended to be used for off-line planning and design purposes. Others are claimed to be suitable for online monitoring and assessment of the system stability. The following section presents a brief overview of some of the most popular voltage stability analysis methods and voltage stability indices that are found in the literature.

2.3 V-P and Q-V Curves

V-P curves, also known as the nose curves, show the relationship between the power injection and the corresponding change in voltage at a particular bus. Figure (2.1) shows a V-P curve. The upper part of the curve corresponds to a stable operating region, while the lower part of the curve corresponds to the unstable region. The tip of the "nose curve" is known as the stability limit. These curves are obtained through the use of continuation power flow. At the voltage stability limit the Jacobian matrix of power flow equations becomes singular and the regular power flow solution does not converge. The continuation power flow overcomes this problem by reformulating the load-flow equations so that they remain well-conditioned at all possible loading conditions. This allows the solution of the load-flow problem for stable, as well as unstable equilibrium points (that is, for both upper and lower portions of the V-P curve).

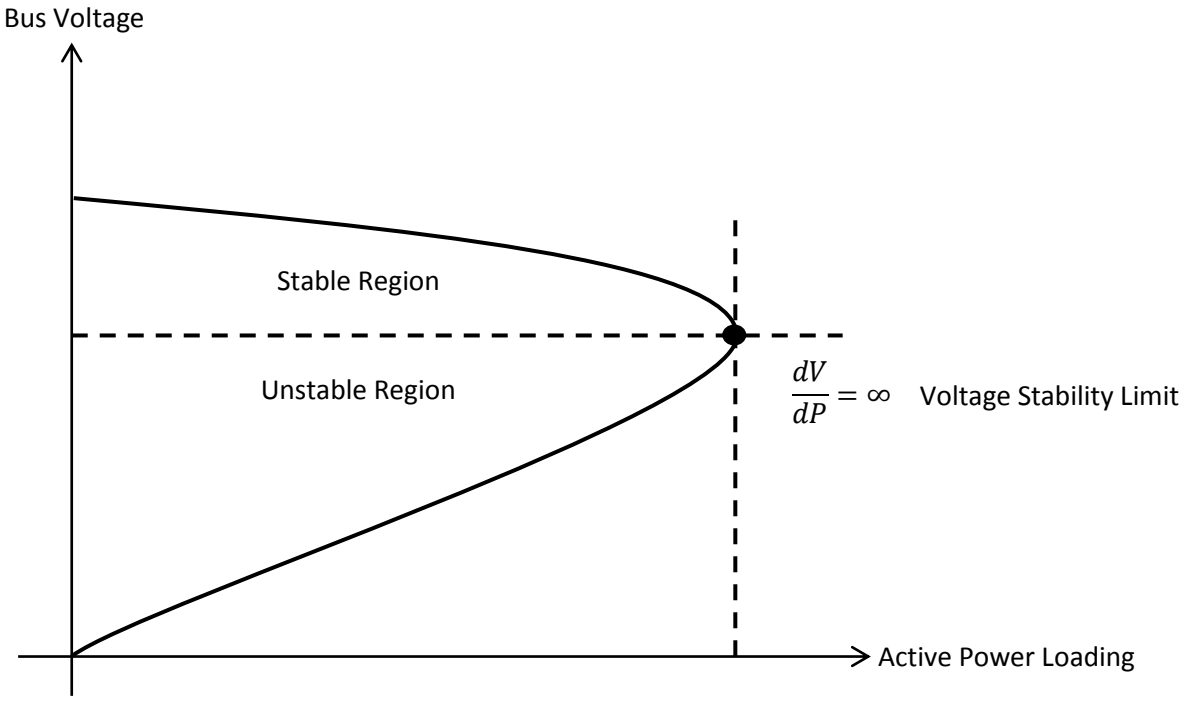

Figure 2.1 P-V Curve

Another useful characteristic for voltage stability analysis is the Q-V curves. These curves show the sensitivity and variation of bus voltages with respect to reactive power injections. Figure (2.2) shows a Q-V curve. The bottom of the curve where dQ/dV is equal to zero represents the voltage stability limit. The right hand side of the curve is stable since an increase in Q is accompanied by an increase in V. The left hand side is unstable since an increase in Q represents a decrease in V.

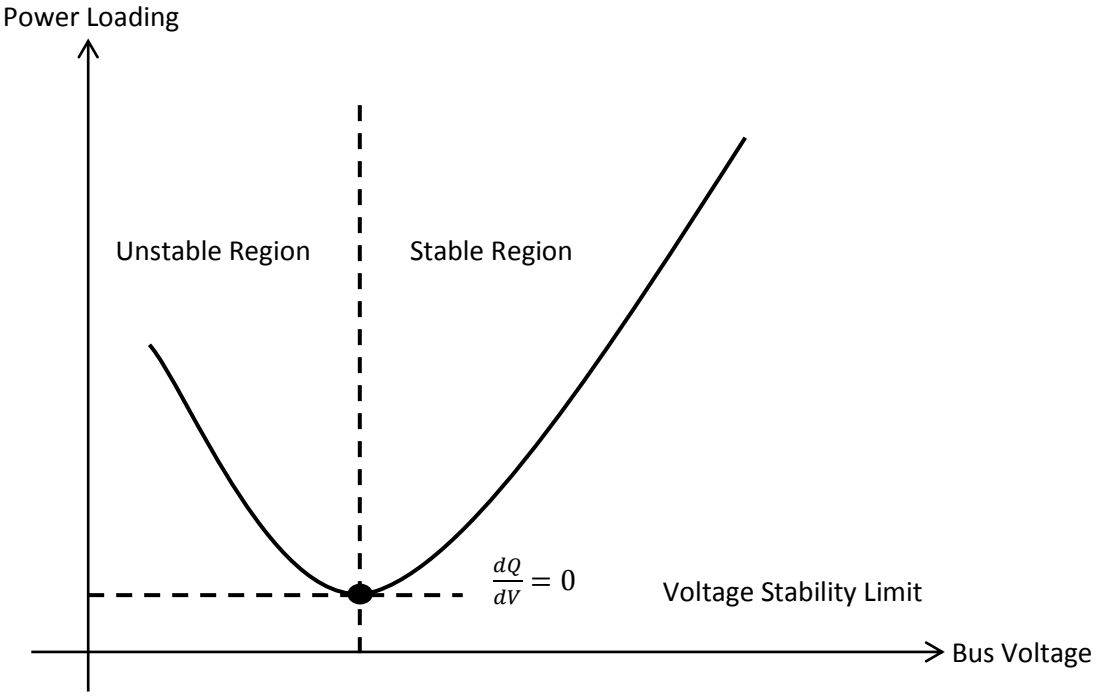

Figure 2.2 Q-V Curve

P-V and Q-V curves are one of the most considered methods to find active power margin and reactive power margin. However, the main disadvantage of these curves is the fact that for many different operating points and contingencies a large number of such curves would be required to obtain complete information on the voltage stability of the whole system. Each one of those curves is

generated by executing a large number of power flows. This makes them very time-consuming and hence not practical for on-line voltage stability monitoring of large power systems.

2.4 Modal Analysis

Modal analysis is a mathematical tool that is used to study the stability of a process or a system. In [2] a V-Q sensitivity analysis method using the modal approach is proposed. The proposed method gives an indication not only of the proximity of the system to voltage collapse but also of the key contributing factors to instability such as the weakest or critical buses and transmission branches. In this method, voltage stability characteristics are determined from the eigenvalues and eigenvectors of the reduced Jacobian matrix which relates the reactive power flow to the changes in bus voltages. Given the Jacobian matrix **J** of a system

$$J = \begin{bmatrix} J_{P\theta} & J_{PV} \\ J_{Q\theta} & J_{QV} \end{bmatrix} \tag{2.1}$$

The reduced Jacobian matrix relating the changes in reactive power flow to the changes in bus voltages is given by

$$J_R = \left[J_{QV} - J_{Q\theta} J_{P\theta}^{-1} J_{PV}\right] \tag{2.2}$$

A positive eigenvalue $\lambda_i > 0$ means that the voltage and reactive power variations of mode i are along the same direction which indicates voltage stable mode. If the eigenvalue is negative $\lambda_i < 0$, then voltage and reactive power variations are along opposite direction and the system is voltage unstable. if $\lambda_i = 0$ then any small change in that modal reactive power would result in infinite changes in the modal voltage and it collapses. The magnitude of the eigenvalue determines the degree of stability. Information concerning the mechanism of voltage instability can be obtained from the left and right eigenvectors corresponding to the critical modes in the system.

2.5 Voltage Stability Indices

Voltage stability indices aim to quantify proximity to voltage collapse. Several voltage stability indices have been developed based on the fact that the system Jacobian matrix becomes singular at the point of voltage collapse. In [3], the minimum singular value of the power flow Jacobian matrix has been used as a static voltage stability index. However, this index shows a very non linear behavior near the collapse point and in the presence of system control limits such as generator excitation limits. To overcome this problem several methods have been proposed. In [4], a voltage stability index known as the second order index is proposed. This index is based on the maximum singular value of the inverse Jacobian matrix and its derivative with respect to the total system load. However, this index is computationally expensive, especially for very large power systems as several matrix and vector manipulations are required. Another index which is based on the system Jacobian matrix is proposed in [5]. It uses the system tangent vector which contains the sensitivities of the system states (voltage magnitudes and angles) to a change in the load. The idea behind the index is based on the fact that as the system approaches the point of collapse the change in a bus voltage with respect to load approaches infinity. However, different systems will exhibit dissimilar tangent vectors for the same proximity to collapse as it is evident from the PV curves. This stability index suffers from the absence of a clear indication that conveys the sense of absolute stability.

In a parallel line of research, the idea of simplifying the whole network to a Thevenin equivalent became very popular especially with the advance in phasor measurement technology. Thevenin equivalent is known to be very simple and straight forward for stability analysis which makes it very suitable for use in real-time power system monitoring. Several voltage stability indices have been developed using the Thevenin equivalent concept. In [6] an index is proposed based on the power transfer impedance-matching principle. This principle states that when the magnitude of the load impedance becomes equal to the magnitude of the Thevenin's impedance, the system reaches the

maximum deliverable power and voltage collapse occurs. The concepts of the Thevenin's equivalent is also used in [7], where instead of the "impedance margin," the authors express the proximity to collapse in terms of the power margin.

Although Thevenin equivalent attracts a great deal of attention, it is not free of difficulties. Tracking of the Thevenin equivalence parameters based on real time measurements proves to be a challenge. In order to compute the Thevenin equivalence parameters at least two measurement sets (snapshots) of local voltage and current phasors are required. Usually more than two snapshots are used in order to eliminate errors and bad measurements. In that case, the Thevenin equivalence parameters are estimated by using the least square method. However, the Thevenin parameters have to be estimated from measurements gathered over a time window that is wide enough for the operating conditions to change, but narrow enough to satisfy the condition of no disturbance on the system side. Unfortunately, this condition can never be satisfied.

Since the Thevenin equivalence parameters are not easy to track, some researchers proposed other on-line voltage stability assessment indices and methods without the identification of the Thevenin equivalence parameters. Some of these indices are based on local measurements of transmission line phasors. In [8] a voltage stability index is proposed based on the idea that the system will collapse if a line reaches its maximum power transfer limit. However, it has been proved in [9] that a single line reaching its maximum power transfer limit is not a sufficient condition for the system voltage to collapse. It is even possible for several lines to reach their limit before the whole system collapses. In [10] another index is proposed based on the fact that near the system point of collapse, the increase in the apparent power at the sending end of a line will no longer yields an increase in the apparent power at the receiving end of that line. However, it has been proved in [11] that this concept holds true if and only if the real and imaginary parts of the load impedance are equal to those of the line impedance.

One of the most popular indices which do not depend on a Thevenin equivalent and is well suited for online applications is the L-index. The L-index is proposed in [12]. It is simple and can easily be calculated from normal load flow data. This index is used in this work for comparison purposes and therefore, a brief overview of it is presented next.

According to the authors in [12], the transmission system can be represented in terms of a hybrid (H) matrix as follows

$$\begin{bmatrix} V_L \\ I_G \end{bmatrix} = [H]. \begin{bmatrix} I_L \\ V_G \end{bmatrix} = \begin{bmatrix} Z_{LL} & F_{LG} \\ K_{GL} & Y_{GG} \end{bmatrix} \begin{bmatrix} I_L \\ V_G \end{bmatrix} \tag{2.3}$$

Where

V_L and I_L are vectors of voltages and currents at load buses.

V_G and I_G are vectors of voltages and currents at generator buses.

Z_{LL}, F_{LG}, K_{GL}, and Y_{GG} are submatrices of the H-matrix. F_{LG} is the matrix of interest for calculating the L-index and it can be found from the system Y-matrix as follows

$$F_{LG} = -[Y_{LL}]^{-1}[Y_{LG}] \tag{2.4}$$

The L-index is defined according to this system representation. For any load bus j, the value of the L-index is:

$$L_j = \left| 1 + \frac{V_{oj}}{V_j} \right| \tag{2.5}$$

Where V_{oj} is the no-load voltage at bus j and it is calculated according to the following equation

$$V_{oj} = -\sum_{i=1}^{ng} F_{ji} \, . \, V_i \tag{2.6}$$

The value of the system L-index is taken to be the maximum value among all load buses. The system L-index varies from 0 at no-load to 1 at the system point of collapse.

2.6 Load Shedding

Under Voltage Load Shedding (UVLS) is one of the mitigation actions for voltage instability. Load shedding is considered a very cost-effective solution for preventing widespread system collapse especially since voltage collapse is a low probability-high impact phenomenon.

The load-shedding schemes proposed in the literature can be classified into two categories. In the first one, the amount of load to be shed is fixed a priori. In other words, when there is a system disturbance and the voltage drops to a pre-selected level for a pre-determined time, then selected loads are shed. The location and amount of load to be shed is usually pre-determined through extensive off-line investigations using dynamic time simulation analysis or static analysis such as V-P and Q-V curves.

In the second category, the amount of load to be shed is determined using optimal power flow techniques. In the literature of load shedding, a great deal of attention has been given to what is known as meta-heuristic optimization techniques, such as genetic algorithm (GA), particle swarm optimization (PSO), ant colony optimization (ACO) … etc to solve the optimization problem of load shedding. Reference [13] provides an overview of all the meta-heuristic methods implemented for under voltage load shedding in power systems.

CHAPTER 3

DEVELOPMENT OF THE PROPOSED VOLTAGE STABILITY INDEX: CONCEPTS AND FORMULAS

3.1 The P-index; a Voltage Stability Indicator

3.1.1 Two bus system

A simple radial system is used at first to explain the concept behind the proposed indicator. Consider the two bus system shown in Figure (3.1) where the load at bus 2 is $P_L + jQ_L$ and the voltage magnitude is V . The equivalent load admittance is $G_L - jB_L$, where

$$G_L = \frac{P_L}{V^2},\ B_L = \frac{Q_L}{V^2} \tag{3.1}$$

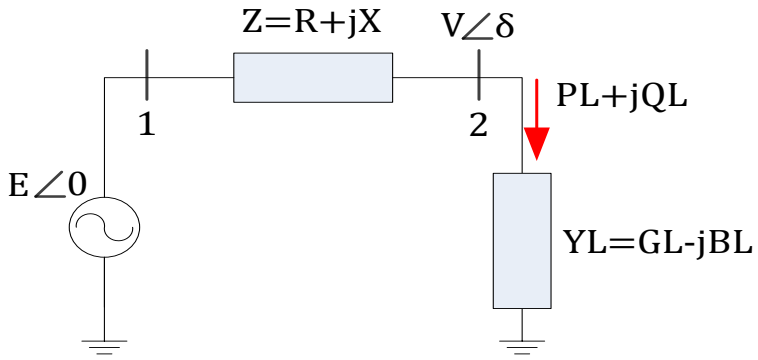

Figure 0.1 Two Bus System

Now let the load be incrementally increased without a change in its power factor by amounts $\Delta P_L, \Delta Q_L$. The corresponding increase in admittance components are $\Delta G_L, \Delta B_L$. The additional loading will cause the voltage to drop by an amount ΔV which is negative, taking the new bus voltage to be $V + \Delta V$. The active power increment at the bus can now be expressed as:

$$\begin{aligned} \Delta P_L &= (V + \Delta V)^2 (G_L + \Delta G_L) - V^2 G_L \\ &= (V + \Delta V)^2 \Delta G_L + (2V + \Delta V) G_L \Delta V \end{aligned} \tag{3.2}$$

The physical significance of the two terms in Equation (3.2) is as follows: the first term (which is positive) represents the power gained due to connection of the additional load ΔG_L, while the second term (negative) is the power lost on original load G_L due to voltage drop ΔV. The net active power gained at the bus is the balance of these opposing terms. At the point of stability limit these two terms cancel out and there is zero net power increase. This point represents the maximum power possible on the V-P curve of the continuation power flow. Any further attempt to increase the power by connecting additional admittance $\Delta G_L, \Delta B_L$ will actually result in a net reduction in power as the second term gains dominance over the first. This represents operation in the lower (unstable) half of the continuation power curve.

The new voltage stability index to be proposed is based on the ratio of the two terms in Equation (3.2), i.e. the ratio of power lost to power gained. A minus sign is introduced to make the index positive when there is a negative voltage drop for positive ΔG_L:

$$P_{index} = -\frac{(2V + \Delta V) G_L}{(V + \Delta V)^2} \cdot \frac{\Delta V}{\Delta G_L} \tag{3.3}$$

In the limiting case as ΔG_L, $\Delta V \to 0$

$$P_{index} = -\frac{2G_L}{V} \cdot \frac{dV}{dG_L} \tag{3.4}$$

The quantity dV/dG_L is not usually encountered in network terminology but can easily be expressed in terms of system power and voltage sensitivities. If dV/dG_L is written as

$$\frac{dV}{dG_L} = \frac{dV}{dP_L} \cdot \frac{dP_L}{dG_L} \tag{3.5}$$

then, using $P_L = V^2 G_L$, one may write

$$dP_L = V^2 dG_L + 2VG_L dV \tag{3.6}$$

Or

$$\frac{dP_L}{dG_L} = V^2 + 2VG_L \frac{dV}{dG_L} \tag{3.7}$$

Substituting in (3.5)

$$\frac{dV}{dG_L} = \frac{dV}{dP_L}\left(V^2 + 2VG_L \frac{dV}{dG_L}\right) \tag{3.8}$$

Which, after manipulations may be expressed as

$$\frac{dV}{dG_L} = \frac{V^2 \frac{dV}{dP_L}}{1 - 2VG_L \frac{dV}{dP_L}} \tag{3.9}$$

Substituting in the P_{index} defined in (3.4),

$$P_{index} = \frac{-2VG_L \frac{dV}{dP_L}}{1 - 2VG_L \frac{dV}{dP_L}} \tag{3.10}$$

Or, in terms of active power,

$$P_{index} = \frac{-2\frac{P_L}{V}\frac{dV}{dP_L}}{1-2\frac{P_L}{V}\frac{dV}{dP_L}} \tag{3.11}$$

The index is now defined in terms of the normalized voltage and power sensitivities. The stability index has a theoretical value of 1.0 at the stability limit when $dV/dP_L = \infty$

It is not a difficult matter to calculate dV/dP_L for the two bus system of Figure (3.1). The calculation involves taking the partial derivatives of active and reactive power equations with respect to both voltage and angle and eliminating the latter derivative. To make elimination possible, the reactive power is expressed in terms of active power using the constant power factor. A general method for finding dV/dP_L will be described in the following section. A plot of bus voltage V versus bus active power P is shown in Figure (3.2) with $E = 1.0$ p.u., $Z = 0.01 + j0.2$ p.u., and a load power factor of 0.8, lagging. On the same plot the corresponding P-index variation is drawn.

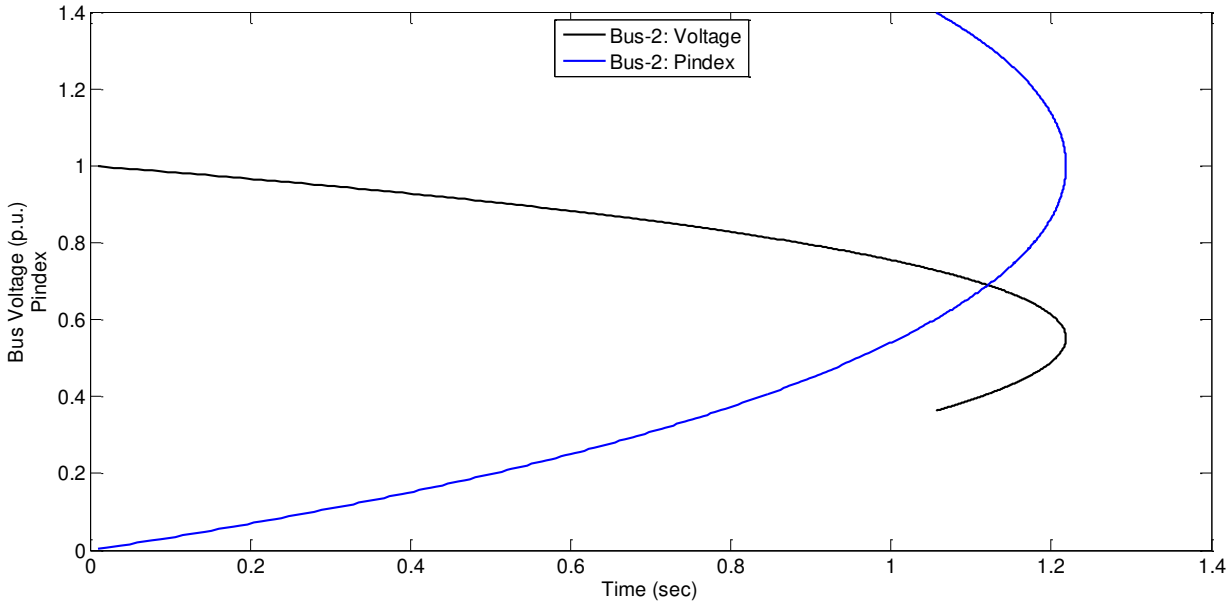

Figure 0.2 Bus-2 Voltage and P-index

3.1.2 General n-bus system

In order to calculate the P-index as defined in (3.11) for every load bus *j* in a general n-bus power network, it is necessary to find the value of dV_j/dP_{Lj}. This can be calculated from the system Jacobian matrix as follows:

Assuming that the system loading was increased from some initial loading $P_{L0\,j}$, $Q_{L0\,j}$ in a manner consistent with the continuation load flow, i.e. through multiplying the system initial loads with a loading multiplier λ, to values P_{Lj} and Q_{Lj}. Let this load then be incrementally increased by ΔP_{Lj} and ΔQ_{Lj}.

If the inverse Jacobian matrix equations are defined as follows,

$$\begin{bmatrix} \Delta\delta \\ \Delta V \end{bmatrix} = \begin{bmatrix} H & N \\ J & L \end{bmatrix} \cdot \begin{bmatrix} \Delta P_L \\ \Delta Q_L \end{bmatrix} \tag{3.12}$$

We may write, for load bus *j*:

$$\Delta V_j = \sum_{\substack{i\in L \\ i\in G}} j_{ji}\Delta P_{Li} + \sum_{i\in L} l_{ji}\Delta Q_{Li} \tag{3.13}$$

Or

$$\frac{\Delta V_j}{\Delta P_{Lj}} \to \frac{dV_j}{dP_{Lj}} = \sum_{\substack{i\in L \\ i\in G}} j_{ji}\alpha_{ji} + \sum_{i\in L} l_{ji}\alpha_{ji}\beta_i \tag{3.14}$$

Where

$\alpha_{ji} = \dfrac{\Delta P_{Li}}{\Delta P_{Lj}} = \dfrac{P_{L0i}}{P_{L0\,j}}$, assuming the load increments are in the same proportion of their initial loading.

$\beta_i = \dfrac{\Delta Q_{Li}}{\Delta P_{Li}} = \dfrac{Q_{L0i}}{P_{L0i}} = \tan\phi_i$, where ϕ_i is the power factor angle of the load at bus *i*.

It is relevant to point out that load bus increments will take a negative sign, while generator bus increments will be positive. The P-index for load bus *j* is then:

$$P_{index-j} = \frac{-2\dfrac{P_{Lj}}{V_j}\dfrac{dV_j}{dP_{Lj}}}{1-2\dfrac{P_{Lj}}{V_j}\dfrac{dV_j}{dP_{Lj}}} \tag{3.15}$$

It must be emphasized that G_L and B_L are just equivalent admittance elements that satisfy the power voltage equations at any loading point P_L and Q_L. Using them as such does not imply that the actual loading is an impedance model. It may be a motor load, a constant current load, or a thermostatic load. The P index is developed from fundamental load flow and Jacobian matrix concepts and serves as such to indicate system performance upon incremental changes in P_L and Q_L for whichever type of load. The only binding assumption is that the power factor remains constant, which is the same constraint followed in developing the nose curves.

The index which comes closest to the P-index is the tangent vector stability indicator $dV/d\lambda$ [5]. Indeed the P-index may be expressed in terms of the tangent vector by substituting $P_{Lj} = \lambda \cdot P_{L0\,j}$; then

$$P_{index-j} = \frac{-2\dfrac{\lambda}{V_j}\dfrac{dV_j}{d\lambda}}{1-2\dfrac{\lambda}{V_j}\dfrac{dV_j}{d\lambda}} \tag{3.16}$$

Unfortunately, the tangent vector as a stability indicator was not originally expressed in terms of normalized sensitivities, making it dependent on the system choice of units or bases. The P-index as defined therefore can be seen as an interesting enhancement of the tangent vector index. Both the P-index and the tangent vector method require knowledge of the system Jacobian matrix to calculate $dV/d\lambda$.

3.2 Application of the P-index to Test Systems and Comparison to the L-index

The first multi-bus test system is the IEEE 14 bus system [14]. The P-index is evaluated for an increase in loading parameter λ on all generator and load buses until the system collapses. The value for $\lambda = 1$ is coincident with the base case. Both the P-index and the L-index select bus 14 as the weakest bus for this system. However while the P-index for bus 14 rises to exactly 1.0 at the loading limit, the L-index fails to reach its presumed theoretical limit of 1.0 and falls behind at 0.66 for the same load. This is shown in Figure (3.3), where the continuation curve of bus 14 is also plotted. This same shortcoming with regards to the L-index was mentioned in [15]. The strongest load bus in the system is bus 12, successfully ranked with the least value by both P and L indices, with the P-index staying at low values right to the verge of collapse where it makes an abrupt turn up to 1.0, as shown in Figure (3.4).

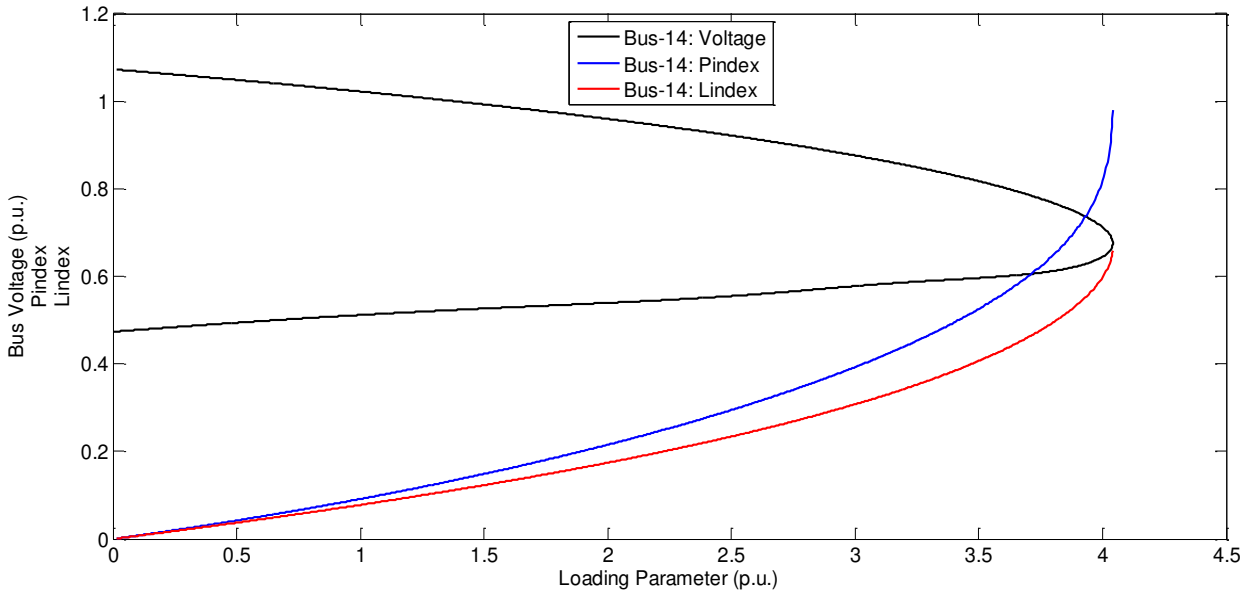

Figure 0.3 Bus-14 Voltage, P-index, and L-index

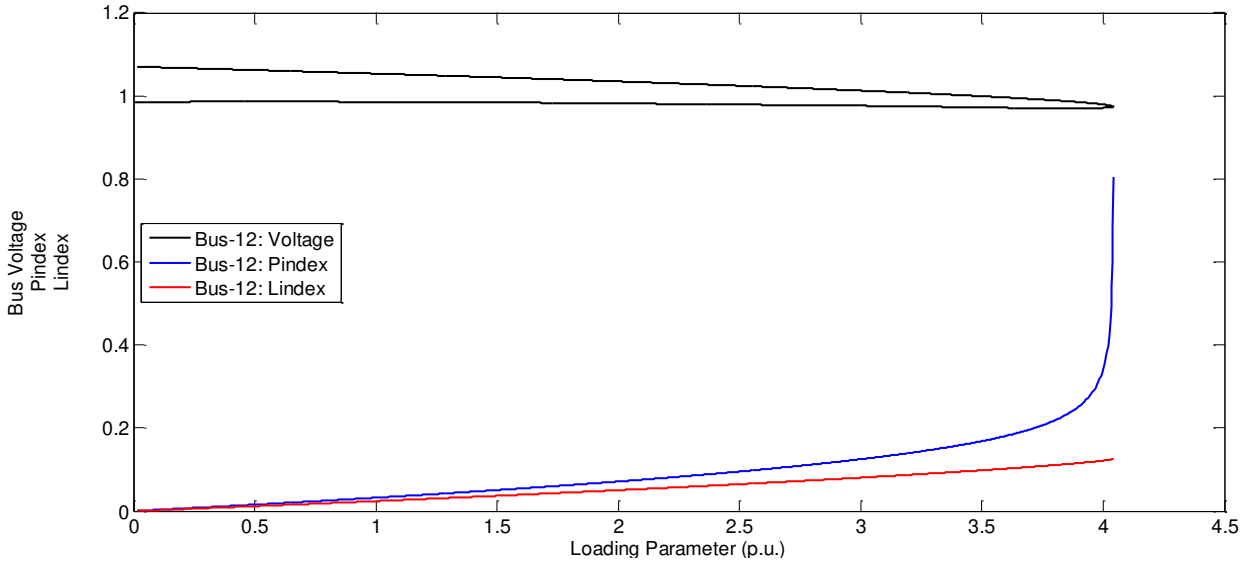

Figure 0.4 Bus-12 Voltage, P-index, and L-index

The complete bus ranking according to both P and L indices is listed in Table (1), computed at P-index = 0.5 for bus 14. It is noted that while the L-index stays consistent with the P-index most of the times, it does make some surprising mis-rankings, as in the case of bus 5, to which it assigns the lowest value although it is among the group of stressed buses according to the P-index. Note also that the P-index is not defined for a load bus with P and Q of zero, as is the case for bus 7.

Table 1 IEEE 14 Bus System Rankings, taken at $\text{P-index}_{14} = 0.5$

Bus No.	**P-index**	**L-index**
14	0.501	0.413
9	0.468	0.346
10	0.452	0.326
5	0.353	0.095
4	0.347	0.137
11	0.294	0.167
13	0.238	0.140
12	0.161	0.099
7	N.A.	0.178

The second test system is the IEEE 57 bus network [14]. Both the P-index and L-index picked bus 31 as the weakest with the highest index score. This time however the L-index greatly exceeds its supposed limit of 1.0 to reach 1.6 as shown in Figure (3.5).

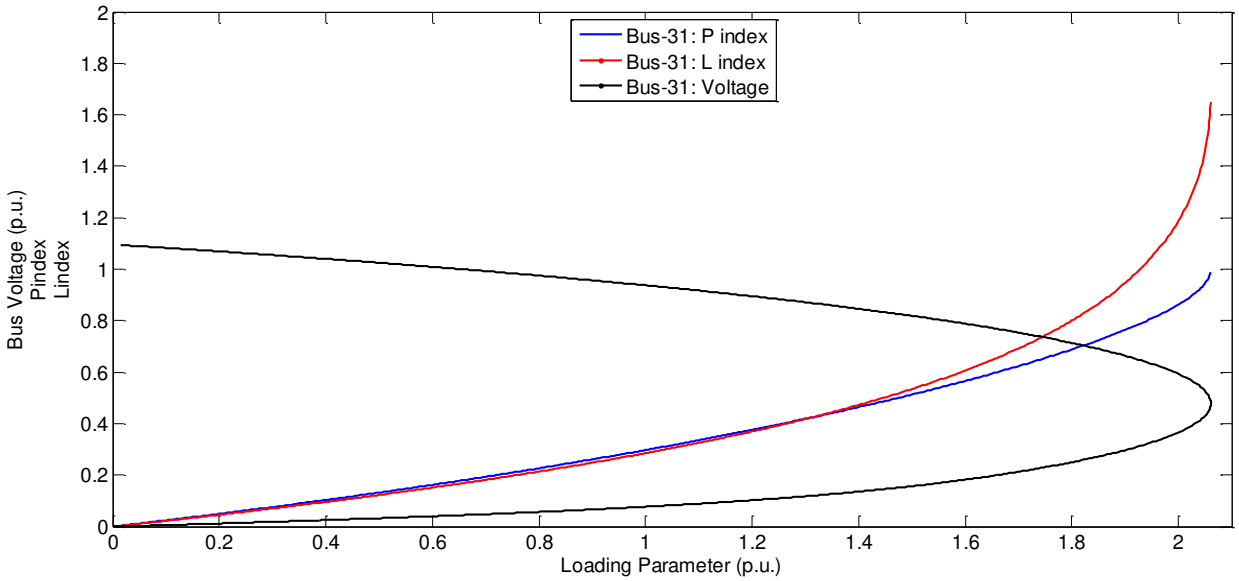

Figure 0.5 Bus-31 Voltage, P-index, and L-index

A comparison of rankings according to the P and L indices for the IEEE 57 bus network is shown in Table 2. The rankings, taken at P-index = 0.5 for bus 31, are mostly consistent with only slight disagreement in some cases.

Table 2 IEEE 57 Bus System Rankings, taken at P-index$_{31}$ = 0.5

Bus No.	P-index	L-index
31	0.501	0.518
33	0.483	0.478
32	0.478	0.472
30	0.438	0.446
25	0.389	0.399
57	0.379	0.337
34	N.A.	0.304
35	0.377	0.286
56	0.360	0.309
40	0.354	0.267
36	0.351	0.264
42	0.341	0.284
39	0.335	0.251
37	0.331	0.248
24	0.310	0.237
26	0.296	0.227
23	0.279	0.212
22	0.275	0.209
21	0.273	0.210
38	0.267	0.201
20	0.248	0.210
48	0.242	0.183
44	0.241	0.177
41	0.239	0.196
47	0.232	0.177
50	0.228	0.175
49	0.218	0.168
53	0.211	0.171
19	0.208	0.194
27	0.208	0.165
52	0.188	0.150
46	0.179	0.126
28	0.154	0.125
45	N.A.	0.102
43	0.144	0.092
14	0.139	0.078
54	0.136	0.110
29	0.109	0.097
51	0.109	0.093

13	0.103	0.056
15	0.099	0.049
11	0.094	0.050
18	0.075	0.133
17	0.075	0.043
10	0.073	0.053
16	0.058	0.038
7	0.051	0.039
55	0.025	0.041
5	0.023	0.015
4	0.022	0.015

3.3 P-index as an Absolute Stability Performance Indicator and Distance to Voltage Collapse

3.3.1 Absolute stability performance

Because the P-index is based on normalized sensitivities, it can better estimate the absolute voltage-power trend from snapshot measurements when compared to other indices. For example, if the P-index has a value of 0.5, this will result in the normalized sensitivity $\frac{dV_j}{V_j} / \frac{dP_j}{P_j}$ of -0.5. This can be used to state that, if the measured trend stays approximately constant, a 10% increase in the load will result in a 5% drop in voltage. This voltage drop is somewhat conservative, as the increasing negative slope will result in a larger drop, but at least it establishes a definite lower limit which may be used to take action. A P-index of 0.66 will result in a more serious state of affairs, with $\frac{dV_j}{V_j} / \frac{dP_j}{P_j}$ now at -1, indicating a voltage drop of at least 10% for a 10% increase in power. Again these trends are to be taken as indicative only of the most conservative outcomes, since the actual slope is system dependent and additionally involves how the aggregate loads will behave under voltage drops, and how they may not necessarily follow a constant power factor pattern.

With regards to using the P-index as an absolute indicator of voltage stability, the performance at a value of P-index = 0.5 was evaluated for the weakest buses of both IEEE 14- and 57-bus systems. For the IEEE 14-bus system, the voltage of bus 14 goes down by 6.27% for a 10% increase in system loading. The IEEE 57-bus systems exhibits a more gradual slope of voltage decline for bus 31 at P-index = 0.5 and yields a voltage drop of 5.16% for a 10% load increase. This is very close to the predicted minimum voltage drop.

3.3.2 Distance to voltage collapse

In reference [12], the authors used the L-index to extrapolate the distance to voltage collapse. To be able to find a non-iterative solution for the maximum value of λ they put forward particular assumptions related to the system variables. In this work, it is shown that the P-index is likewise capable of finding the approximate collapse point if the quantity dV/dG_L in Equation (3.4) is assumed constant. Referring to Figure (3.1), the load voltage, which is $\overline{V} = \overline{E} - \frac{\overline{E}}{\overline{Z}_L + \overline{Z}}\overline{Z}$, is approximately equal $\overline{E} - \overline{E}\overline{Z}\frac{1}{\overline{Z}_L}$, or $\overline{E} - \overline{E}\overline{Z}\overline{Y}_L$ for small values of $\bar{Y}_L$ and $\bar{Z}$. Assuming a constant power factor and purely reactive line impedance $\bar{Z} = jX$, we may express the load voltage magnitude as $V = |E - jEXG_L(1 - j\tan\phi)| = |E(1 - G_L X\tan\phi) - jEG_L X|$. The imaginary part is quite small compared to the real part; thus $V \approx E(1 - G_L X\tan\phi)$ leading to $dV/dG_L \approx EX\tan\emptyset$ which is constant. If however either the load conductance G_L or the transmission line reactance X increase significantly the linear relation approximations no longer hold. A more rigorous analysis shows increasing dependency of dV/dG_L on G_L and its higher powers, but these terms are small and gather importance slowly.

Let us investigate to what extent this assumed linearity is true on a larger system. Figure (3.6) shows the $V - G_L$ characteristics of bus 14 for the IEEE 14 bus system, where G_L varies from zero up to

the point of collapse. Part (a) is for the intact system, while part (b) is for an outage of line 13-14. The first graph is clearly linear with a constant slope, while the second exhibits slight 'convex' characteristics. Nevertheless we proceed to examine how use of the assumed constant dV/dG_Lmay help to find the stability limit.

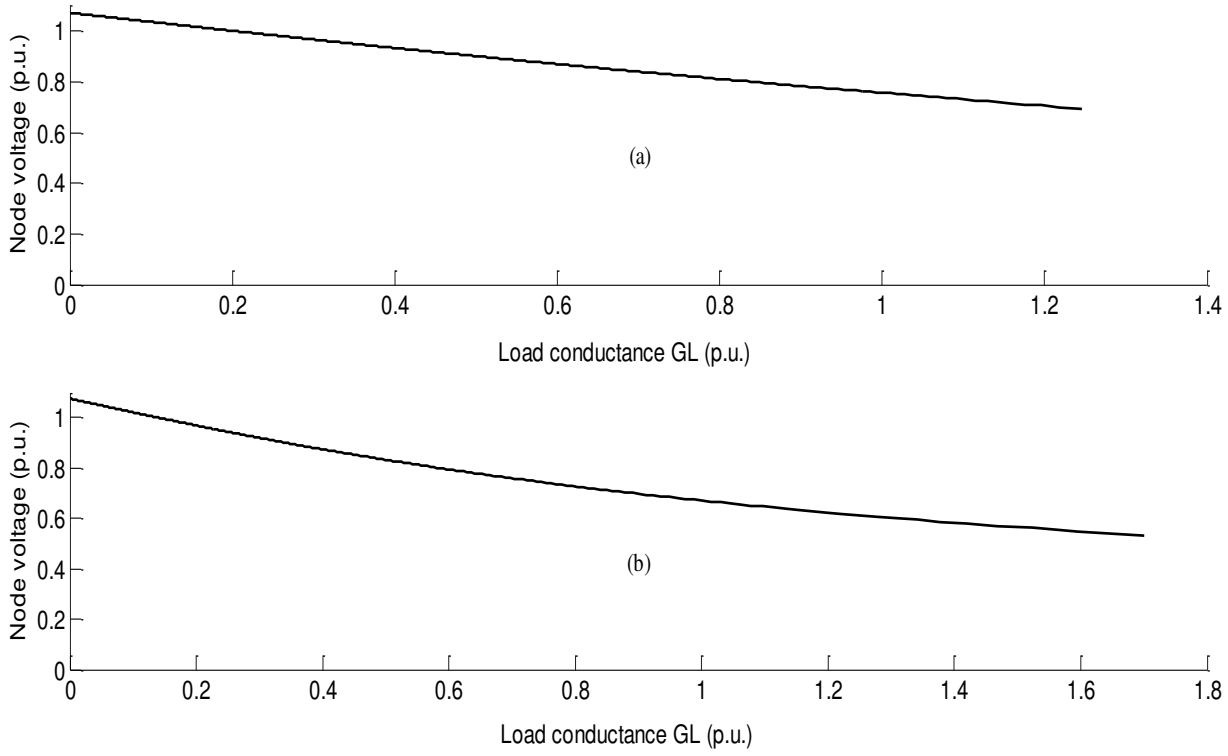

Figure 0.6 Bus-14 V-G_L Characteristics: a) Intact System, b) Line 13-14 Outage

Assume that the system at the current snapshot has acquired a P-index of 0.5 for its most critical node. This is the level that is proposed here to be worthy of raising the alarm indicating proximity to voltage collapse. The slope dV/dG_L may be then calculated using Equation (3.4), with the substitution

of P-index = 0.5, and determining G_L from Equation (3.1). Since we now have a slope and a coordinate pair (G_L, V_L) we may express for the node in question the equation of a straight line as

$$V = aG_L + b \tag{3.17}$$

Where $a = dV/dG_L$ and b are calculated from the conditions at P-index = 0.5

Next we look at Equation (3.4) again for the conditions of voltage collapse at which the P-index = 1.0. This results in another straight line equation passing through the origin

$$V = -2aG_L \tag{3.18}$$

Where a is substituted for dV/dG_L assuming it to remain constant between the measured point and point of collapse.

Solving Equations (3.17) and (3.18) together results in conditions at the point of collapse as

$$V = \frac{2}{3}b, \text{ and } G_L = -\frac{b}{3a} \tag{3.19}$$

And the power at the point of collapse

$$P_{L-\max} = V^2 G_L = -\frac{4b^3}{27a} \tag{3.20}$$

Which, when substituting the original measurements taken at P-index=P_{idx1} becomes

$$P_{L-\max} = -\frac{4}{27}\left(V(P_{idx1}) - \frac{dV}{dG_L}G(P_{idx1})\right) \Big/ \frac{dV}{dG_L} \tag{3.21}$$

Equation (3.21) may be manipulated as follows:

$$P_{L-\max} = -\frac{V^2(P_{idx1})\cdot G_L(P_{idx1})}{27}\left(2 - 2\frac{dV}{dG_L}\frac{G_L(P_{idx1})}{V(P_{idx1})}\right)^3 \Big/ 2\frac{dV}{dG_L}\frac{G_L(P_{idx1})}{V(P_{idx1})} \tag{3.22}$$

Or (noting that $P_L(P_{idx1}) = V^2(P_{idx1}) \cdot G_L(P_{idx1})$):

$$P_{L-\max} = \frac{1}{27} P_L(P_{idx1}) \cdot \frac{\left(2 + P_{idx1}\right)^3}{P_{idx1}} \tag{3.23}$$

In terms of λ,

$$\lambda_{\max} = \frac{1}{27} \lambda(P_{idx1}) \cdot \frac{\left(2 + P_{idx1}\right)^3}{P_{idx1}} \tag{3.24}$$

If the collapse point is estimated when the P_{idx1} is 0.5 then the estimate for λ_{max} will be $1.157\ \lambda_{(0.5)}$. Therefore a system which exhibits fairly linear $V - G_L$ behavior will be expected to have a 16% load margin to collapse when its P-index measures 0.5.

Using Equation (3.23), with the data at node 14 at P-index=0.5, the point of collapsed for the IEEE 14 bus was predicted to be at $\lambda = 3.89$ for the intact system and $\lambda = 2.76$ for the system with an outage of line 13 – 14. The corresponding exact values are 4.04 and 3.24, constituting errors of 3.7% and 15%. The large error in the latter case is clearly attributed to the non-linear $V - G_L$ behavior discussed above.

The estimate can of course be improved by repeating the above process using the last estimate as a starting point. If the calculations above are performed iteratively, and stopped when the difference in λ for successive iterations becomes less than 1%, then only 2 iterations are required for the 14 bus system without an outage, and 4 iterations for the case where line 13-14 was outaged.

It must be cautioned however against relying upon using the above method or more accurate refinements as an indicator of the collapse point for practical systems. The assumptions that the loads will move in the same proportion and will have the same aggregate characteristics cannot be guaranteed in reality. However the assumption of constant dV/dG_L can be employed in the more useful

context of load shedding to determine the amount of load to be curtailed for P-index recovery as will be demonstrated.

3.4 Using the P-index for Load-Shedding Purposes

The techniques developed in Section (3.3) can be used to carry out load shedding with the intention of lowering the P-index to a more tolerable value. The case for constant dV/dG_L becomes stronger since the range of variation for G is much smaller than when investigating the distance to collapse. Assume that the P-index is at 0.5 and it is desired to move it back by 0.1 to 0.4 by performing the appropriate load shedding. The first thing to understand is that shedding should be performed at all buses in proportion to their loading since this is the way the P-index is defined. It is possible – for the purposes of load shedding - to define the P-index differently with the intention that only the load at one bus will change. This will only require a slight modification to (3.13) and (3.14) such that incremental power ΔP, ΔQ at all busbars except bus j is set to zero. Thus:

$$\Delta V_j = j_{jj}\Delta P_{Lj} + l_{jj}\Delta Q_{Lj} \tag{3.25}$$

Or

$$\frac{\Delta V_j}{\Delta P_{Lj}} \to \frac{dV_j}{dP_{Lj}} = j_{jj} + l_{jj} \cdot \beta_i \tag{3.26}$$

However we define the P-index, for single bus shedding or for general shedding, the calculation for every bus remains the same. If we move the P-index from P_{idx1} to P_{idx2}, it is easy to verify that the new loading on the bus will be

$$P_L(P_{idx2}) = -\frac{4}{P_{idx2}} \frac{\left(V(P_{idx1}) - \frac{dV}{dG_L} G(P_{idx1})\right)^3}{\left(1+\frac{2}{P_{idx2}}\right)^3} \Bigg/ \frac{dV}{dG_L} \tag{3.27}$$

Equation (3.27) is actually a generalization of (3.21), which is obtained by substituting P_{idx1}=1.0. It can be expressed in terms of original loading $P_L(P_{idx1}) = V^2(P_{idx1}) \cdot G_L(P_{idx1})$ as

$$P_L(P_{idx2}) = P_L(P_{idx1}) \cdot \frac{P_{idx2}}{P_{idx1}} \cdot \left(\frac{2+P_{idx1}}{2+P_{idx2}}\right)^3 \tag{3.28}$$

The amount of load to shed is then

$$\begin{aligned} \Delta P &= P_L(P_{idx2}) - P_L(P_{idx1}) \\ \Delta Q &= \beta \Delta P \end{aligned} \tag{3.29}$$

3.5 Using the P-index for Online Stability Monitoring with PMU Measurements

Some researchers claim that Jacobian-based stability indices are not suitable for online applications because of the lengthy computations required, and that system variable-based indices such as the L-index, or line-based indices are more suitable. However this is only true in the case where multiple power flows are required such as the continuation load flow. The P-index calculation does not even involve a single load flow cycle, and the only elaborate calculation required is the inversion of the Jacobian matrix, which can easily be accomplished in a fraction of a second.

To use the P-index for voltage stability assessments in real-time, systems states and nodal power are required, in addition to the network model. The first step in building the network model is to identify the topology. Several efforts have gone into topology processing for PMU applications [16], [17], [18] and rely chiefly on recognizing breaker status. Transformer tap positions will also need to be included in the PMU analogue channels, as are the status position of switches controlling a bank of

shunt capacitors or reactors at a node. This makes for quite a complex topology processing scheme. In this work, a simple and quick method for recognizing system topological changes is discussed. The method relies on state information and nodal power measurements only, without need to communicate breaker or switch status or transformer tap position. It can further be used on reduced systems, where individual status information for unobserved nodes or lines is absorbed in the aggregation.

The method is based on simulating a line outage between two nodes with fictitious injections to the nodes in a system with no topology modification to represent the outage. The injections are then used to estimate the changes made to the system admittance model to reflect the outage. The origins of the method were discussed in the context of DC load flows for linear systems in [19] but only as models to simulate known outages, rather than to estimate changes to the system model.

3.5.1 Nodal injections and circulating flows

Consider the network line segment shown in Figure (3.7). The segment represents a double-circuit line between nodes i and j. Let an outage occur on one of the circuits, resulting in nodal states $V_i\angle\delta_i$ and $V_j\angle\delta_j$. Now, as shown on the same figure, the line outage may be modelled with the outaged line in service, i.e. with its energizing breakers closed, and with two fictitious injection pairs at its terminals which take up such values that result in the flow across the breakers being zero. These two injection pairs P_{i-inj}, Q_{i-inj} and P_{j-inj}, Q_{j-inj} combine with the loads at the nodes $i$and j to give total node power P_i, Q_i and P_j, Q_j. To calculate the nodal injections resulting from an outage, one must first use the captured system states (V, δ) with the network model to find the nodal power and then subtract the load and/or generation already at the bus to get the balancing injections P_{i-inj}, Q_{i-inj} and P_{j-inj}, Q_{j-inj}.

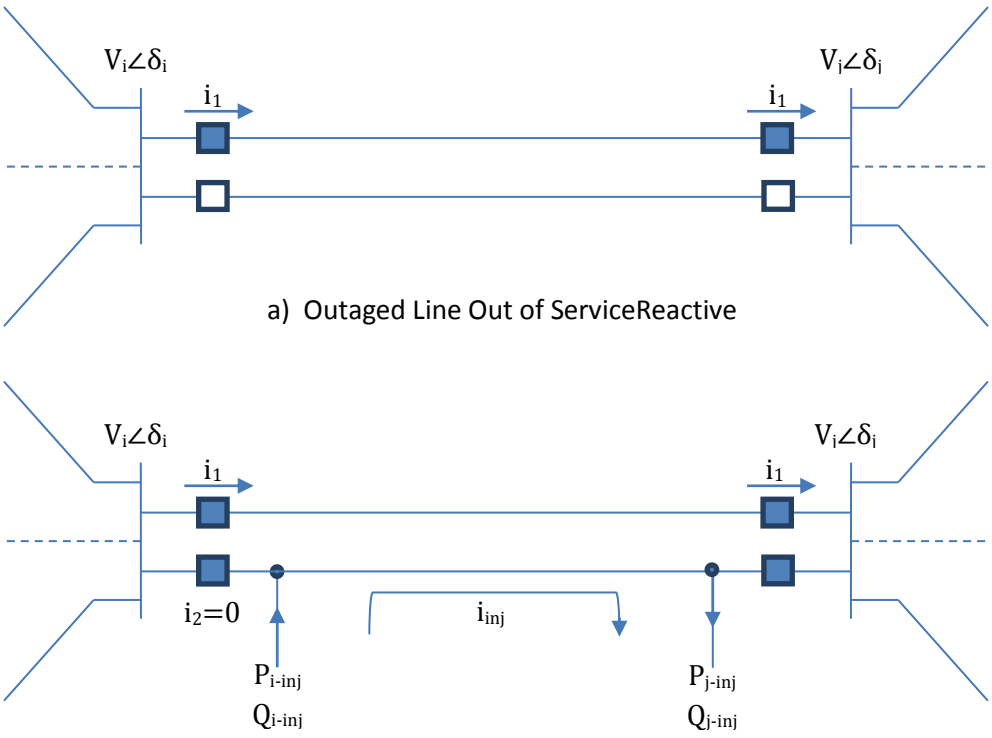

a) Outaged Line Out of ServiceReactive

b) Outaged Line In Service with Power Injections

Figure 0.7 Nodal Injections and Circulating Flows

3.5.2 Estimation of outaged line admittance

Upon calculation of injections and successfully 'pairing' the nodes thought to be involved in an outage event, it becomes possible to estimate the outaged line admittance. An equivalent π model for the line maybe used requiring three admittance values to be estimated; series conductance and susceptance g_L, b_L and shunt half-line charging susceptances b_{sh}(at each end of the line). The power injections for node i are expressed in terms of nodal states and outaged line admittances as follows

$$P_{i-inj} = \left[V_i^2 - V_i V_j \cos(\delta_i - \delta_j)\right] \cdot g_L + V_i V_j \sin(\delta_i - \delta_j) \cdot b_L$$
$$Q_{i-inj} = -V_i^2 \cdot b_{sh} + \left[V_i^2 - V_i V_j \cos(\delta_i - \delta_j)\right] \cdot b_L - V_i V_j \sin(\delta_i - \delta_j) \cdot g_L \quad (3.30)$$

Node j will have identical equations with subscripts i and j interchanged. Since there are four equations for only three unknowns the problem becomes an estimation exercise for the unknown admittance values. We may arrange the equations in a compact form as

$$\begin{bmatrix} P_{i-inj} \\ Q_{i-inj} \\ P_{j-inj} \\ Q_{j-inj} \end{bmatrix} = [H] \cdot \begin{bmatrix} g_L \\ b_L \\ b_{Sh} \end{bmatrix} \tag{3.31}$$

The outaged line admittances are then determined as

$$\begin{bmatrix} g_L \\ b_L \\ b_{Sh} \end{bmatrix} = \left([H]^T \cdot [H] \right)^{-1} \cdot [H]^T \cdot \begin{bmatrix} P_{i-inj} \\ Q_{i-inj} \\ P_{j-inj} \\ Q_{j-inj} \end{bmatrix} \tag{3.32}$$

The calculated admittances should be approximately equal to those of the outaged line. They can thus be used to modify the nodal admittance matrix by subtracting their values from the appropriate corresponding entries within the matrix.

If the outaged element is a transformer, the required admittances become one series susceptance b_{se} and two shunt components b_{sh1}, b_{sh2}. These three elements provide the degrees of freedom required to represent the outaged transformer for any tap position. The calculated elements need not represent an outage condition; they may merely represent the changes needed to reproduce the correct tap position in case it is not available in the PMU measurements.

Finally, if the nodal states are substituted in a system and it resulted in a fictitious injection at one node only, with a failure to pair it with neighboring nodes, then this can point to a load that was not accounted for, a correction to load measurements or an unaccounted for shunt capacitor or reactor that may have been inserted dynamically due to automatic switching.

3.5.3 Pairing outage nodes

Assuming at any given instant only a probable $n-1$ outage, it becomes a relatively easy procedure to identify and pair or associate the nodes between which an outage is probable. First, the states acquired from the PMUs representing a system snapshot are used on the system model to detect any significant nodal injections not accounted for. Given the stochastic nature of the PMU measurements, some spurious bus power mismatches are expected, and therefore a criterion is needed to act upon or ignore detected injections. The criteria could simply be based on a percentage of the system load at the bus, or an absolute value such as 0.1 p.u. power, below which bus power mismatches are ignored. The second step would be to associate nodal pairs as candidates for an outage. Only injections pairs between neighboring nodes are considered. Further the values for real power injections P_{i-inj} and P_{j-inj} should have opposite signs. This is not necessary for reactive powers since the outaged line in the $i-j$ segment might generate sufficient vars to mask the circulation effect under light load conditions, and conversely absorb excessive vars under heavy load conditions. Strictly speaking only one such pair of nodes should be found for an $n-1$ outage probability, but if more than one pair is detected, it could represent a tap change or a previous outage that was not taken into account by updating the system topology.

3.5.4 Reduced topology

There could be parts of the network which are reduced because they are not covered by PMU measurements. It is not possible to calculate the states for these unobserved nodes unless the exact topology is known, and conversely the exact topology cannot be estimated if the states are unknown. However if an outage has occurred in a reduced part of the network, the outage will still be reflected as circulating injections at the boundaries of the reduced portion of the network. If two boundary nodes

form a circulating injection pair, the procedure for estimating correcting the network model is the same as for the non-reduced network. However if more than two boundary circulations are detected, it becomes impossible to estimate the correct topology, as more degrees of freedom are needed. In this situation, the detected injections are simply considered as additional fictitious loads on the system and used as such in the subsequent analysis. Treating injections as loads leads to some inaccuracies in the calculation of the P-index because it assumes that these injections which stem from line flows are proportional to bus nodal power. This is valid for a linear approach such as the DC load flow but is subject to loss of accuracy for ac load flows.

3.5.5 An example for topological change calculations

The IEEE 14 bus system was simulated for an outage of line 13-14 at loading conditions of $\lambda = 1.5$ with reference to base load conditions. The solved states were then substituted in the non-outaged system model and resulted (after subtracting the loads) in injections to nodes 13 and 14 only. These injections were used together with the nodal states to estimate the outaged line parameters. Table (3) lists states and injections for nodes 13 and 14. The calculated admittances are also shown, and are found to be identical to the outaged line parameters. Another outage example is for line 2-3 at the same loading conditions. The results are shown in Table (4). Note that the Q injections for both nodes are positive, indication of the large reactive consumption of the outaged line.

Table 3 Network Modification Results (Line 13-14 Outage)

Nodes	**V (p.u.)**	**δ (rad)**	**P_{inj} (p.u.)**	**Q_{inj} (p.u.)**
13	1.0476	-0.3992	0.2874	0.1819
14	0.9426	-0.469	-0.2694	-0.1452
$g_L = 1.1383$ p.u.		$b_L = 2.3155$ p.u.		$b_{sh} = 0.0$ p.u.

Table 4 Network Modification Results (Line 2-3 Outage)

Nodes	**V (p.u.)**	**δ (rad)**	**P_{inj} (p.u.)**	**Q_{inj} (p.u.)**
2	1.0450	-0.1359	2.9700	0.2840
3	1.0100	-0.7091	-2.5857	1.2426
$g_L = 0.047$ p.u.		$b_L = 0.198$ p.u.		$b_{sh} = 0.0438$ p.u.

CHAPTER 4

RESULTS AND DISCUSSION

Time domain simulation is usually the method of choice to capture the dynamics of voltage stability. It is useful in identifying and studying the various events and their chronology leading to voltage instability and eventually voltage collapse. In this work, time domain simulation is used to verify the adequacy of the proposed P-index in assessing the stability of a system where load dynamics, on-load tap changers and generators' over-excitation limiters are all modeled and accounted for. The system used in this work is the well-known Kundur 10-Bus system [20]. This system is a good testing platform for dynamic voltage stability studies since it incorporates generator controls, tap changer dynamics and various load models. Figure (4.1) shows the one-line diagram for the system. The generators, transmission lines, transformers, and loads data is provided in Appendix A.

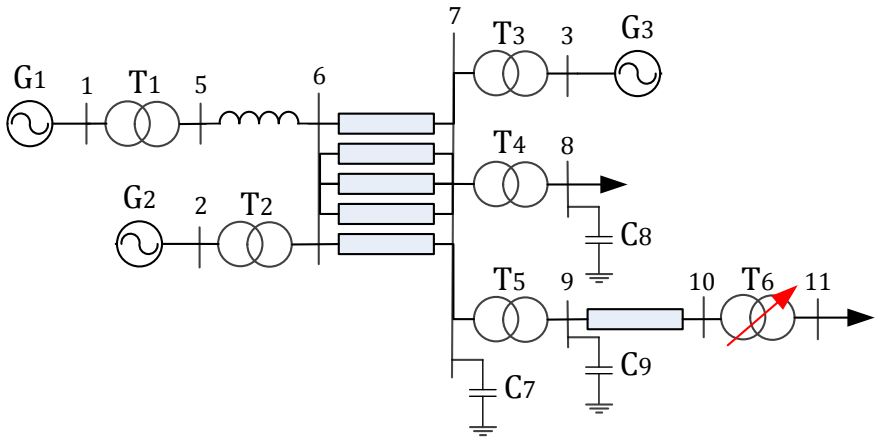

Figure 4.1 Kundur 10-Bus System

4.1 System Modeling

4.1.1 Load dynamics

The active and reactive power components of the load at bus 8 are represented by an equivalent induction motor. The load at bus 11 is modeled as 50% constant impedance and 50% constant current for both active and reactive components.

4.1.2 Transformer on-load tap changer (OLTC)

Transformer T6 is equipped with an OLTC. The time delay for the first tap movement is 30 seconds. For subsequent tap movements, the time delay is set to be 5 seconds. The OLTC has a dead-band equal to ±1% of the controlled bus voltage. Tap range is ±16 steps, with a step *size* equal to 0.625%

4.1.3 Overexcitation limiter (OXL)

Both generators G2 and G3 have static exciters but only generator G3 has an excitation limiter. The block diagram and characteristics of the OXL are shown in Figures (4.2) and (4.3). When the field current exceeds the high setting ($I_{fd\ max2}$), the excitation is reduced instantaneously to limit the field current to a value equal to $I_{fd\ max2}$ and then the current is ramped down within 30 seconds to its continuous limit ($I_{fd\ max1}$). If the field current exceeds the continuous limit but is below the high setting, the current is ramped down to its continuous limit within a time delay dependent on the level of field current and the value of K_1. The OXL parameters are as follows:

$$I_{fd\,max1} = 3.02\ p.u. \qquad K_1 = 0.248$$

$$I_{fd\,max2} = 4.60\ p.u. \qquad K_2 = 12.6$$

$$I_{LIM} = 6.37\ p.u.$$

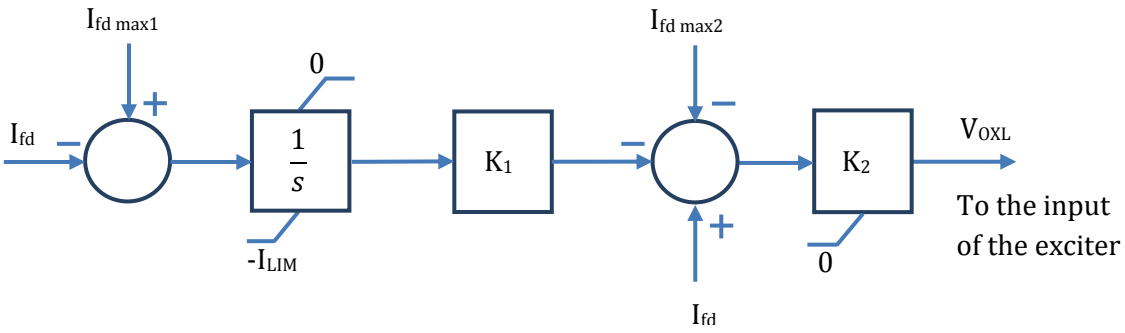

Figure 4.2 OXL Block Diagram

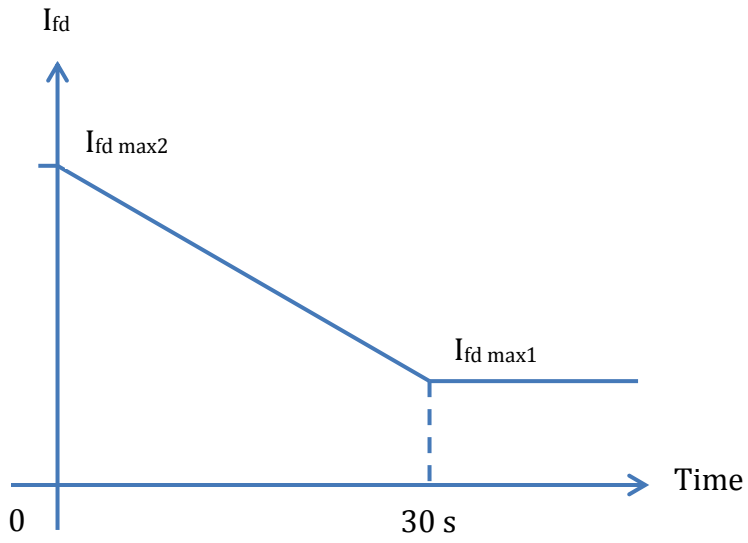

Figure 4.3 OXL Characteristics

4.2 Implementation in Hypersim

Hypersim is a real-time simulation software used for modeling and simulation of power systems. This software has the capability to model the dynamics of power system components such as the voltage dependency of the loads, load tap changer actions, generators excitation and stabilizing systems … etc. In addition, Hypersim allows the user to monitor, control and change some of the system parameters while the simulation is running in real time. In this work, Hypersim is used to simulate a voltage collapse in Kundur 10-Bus test system. Figure (4.4) shows the system model as built in Hypersim

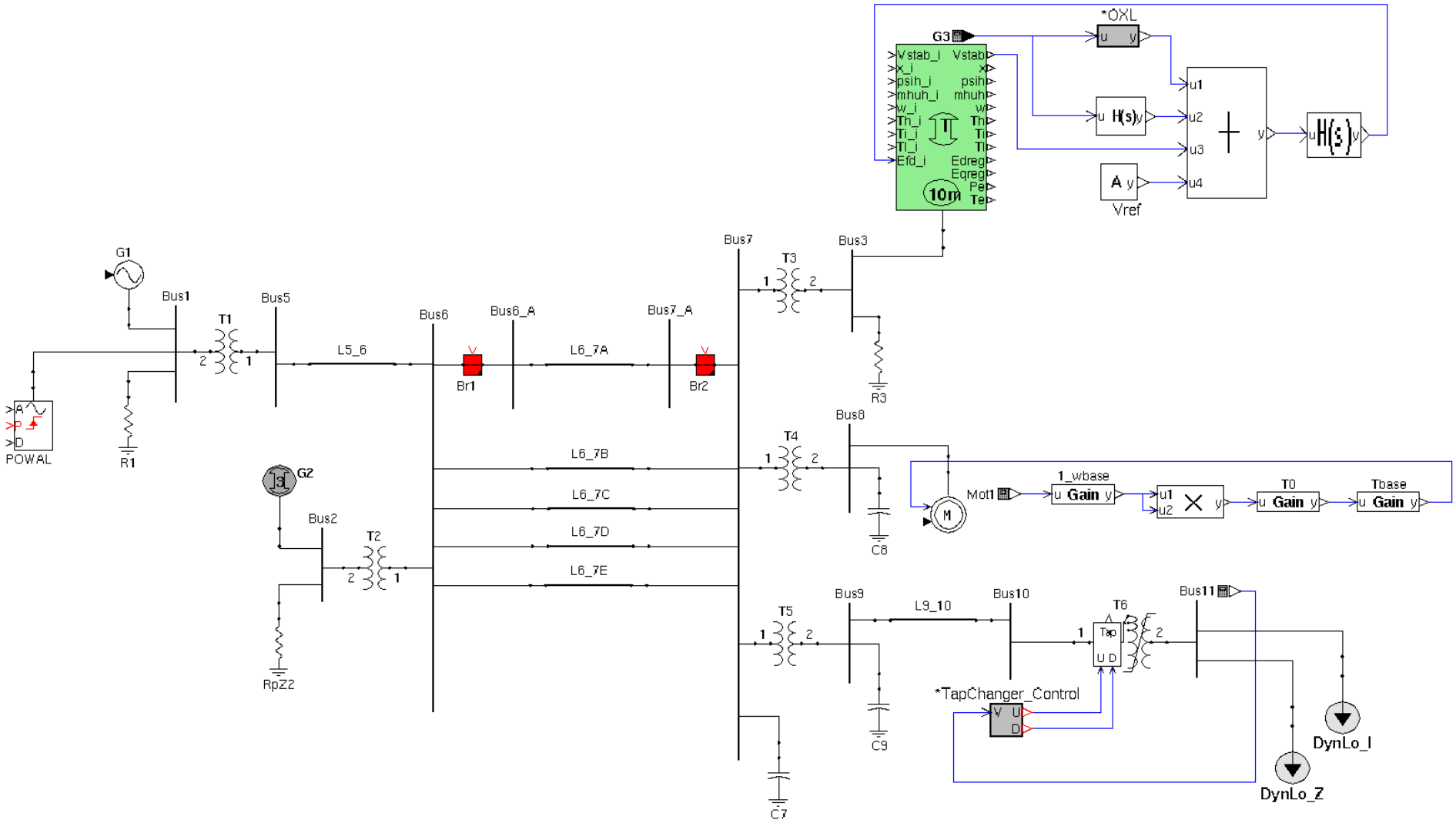

Figure 4.4 Kundur 10-Bus System Model in Hypersim

4.3 Voltage Collapse Simulation Results

The trend towards the eventual voltage collapse is triggered by the loss of one of the transmission lines between buses 6 and 7 (without a fault). Figures (4.5) and (4.6) show the time response of the voltages at bus 8, 10 and 11. The motor active and reactive power are both shown in Figure (4.7) and finally, generator G3 field current, reactive power, and terminal voltage are shown in Figures (4.8), (4.9) and (4.10).

After the transmission line is lost, the system voltage drop and the voltage at bus 11 becomes equal to 0.94 p.u. In order to restore the voltage at bus 11, the OLTC on transformer T6 operates and increases the tap. However, as can be seen from Figure (4.6), the net effect of each tap movement of transformer T6 progresses towards eventually reducing bus 11 voltage rather than increasing it. This reverse action of the OLTC is due to the fact that the system is heavily stressed. The increase in tap position increases the current on the source side of the tap changer. This increase in load current will increase the voltage drop across the weak transmission system thereby decreasing the voltage at the source side of the tap changer, i.e. bus 10. Eventually, the drop caused by the transmission will outweigh the voltage increase due to tap offset.

In addition, the voltage drop at bus 8 causes the motor to draw more current thereby increasing the reactive power consumption of the motor. This will cause the voltage across the transmission system to drop even further. The combined effect of the tap-changer actions and the constant power induction motor persist in stressing the system until it reaches its point of collapse after 58 seconds.

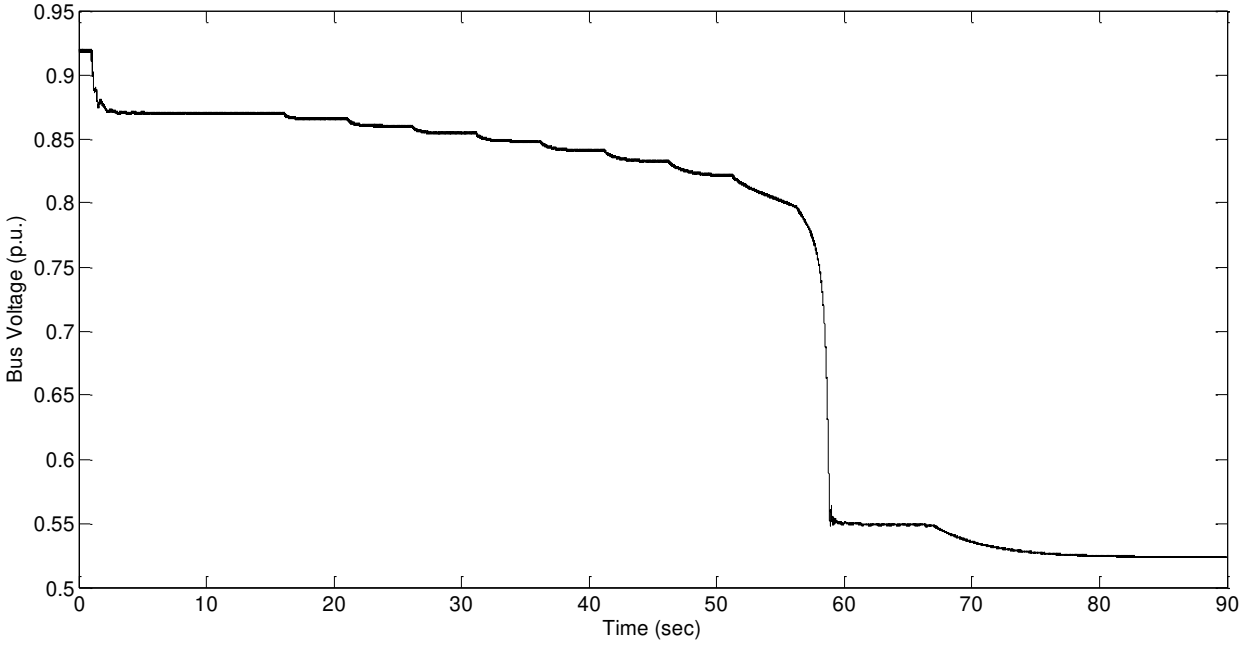

Figure 4.5 Bus-8 Voltage

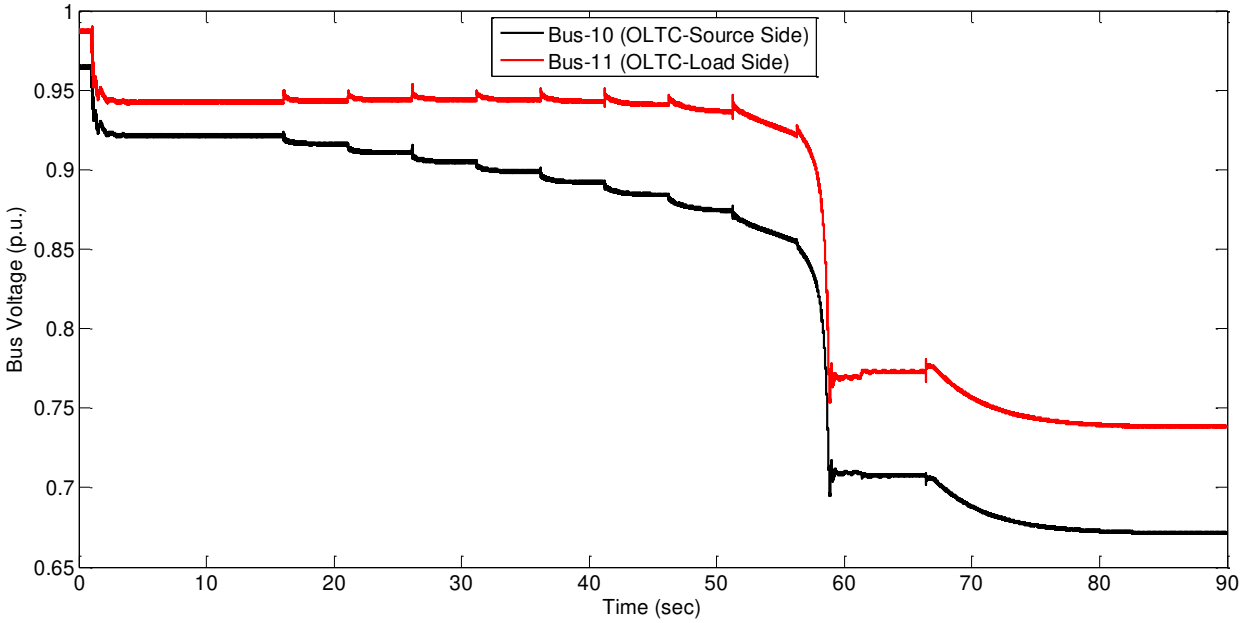

Figure 4.6 Bus-10 and Bus-11 Voltages

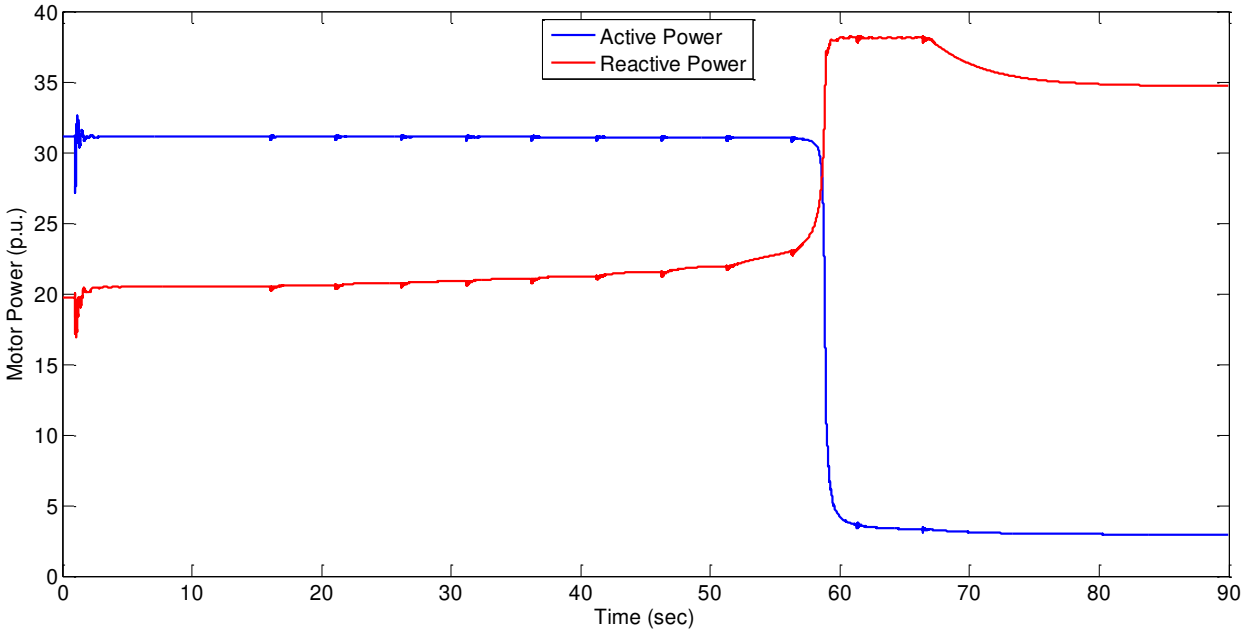

Figure 4.7 Motor Load Active and Reactive Power

It should be noted that after the system collapses, the motor stalls and the active power consumed by the motor greatly decreases. However, the reactive power drawn by the motor increases rapidly and consequently, the field current of G3 reaches its limit. As can be seen from Figure (4.8), the field current reaches a value of 3.6 and after 8 seconds it starts ramping down till it reaches its maximum allowable continuous rating of 3.02 p.u. With the loss of voltage control by G3, the voltage at the transmission and load buses drops even further.

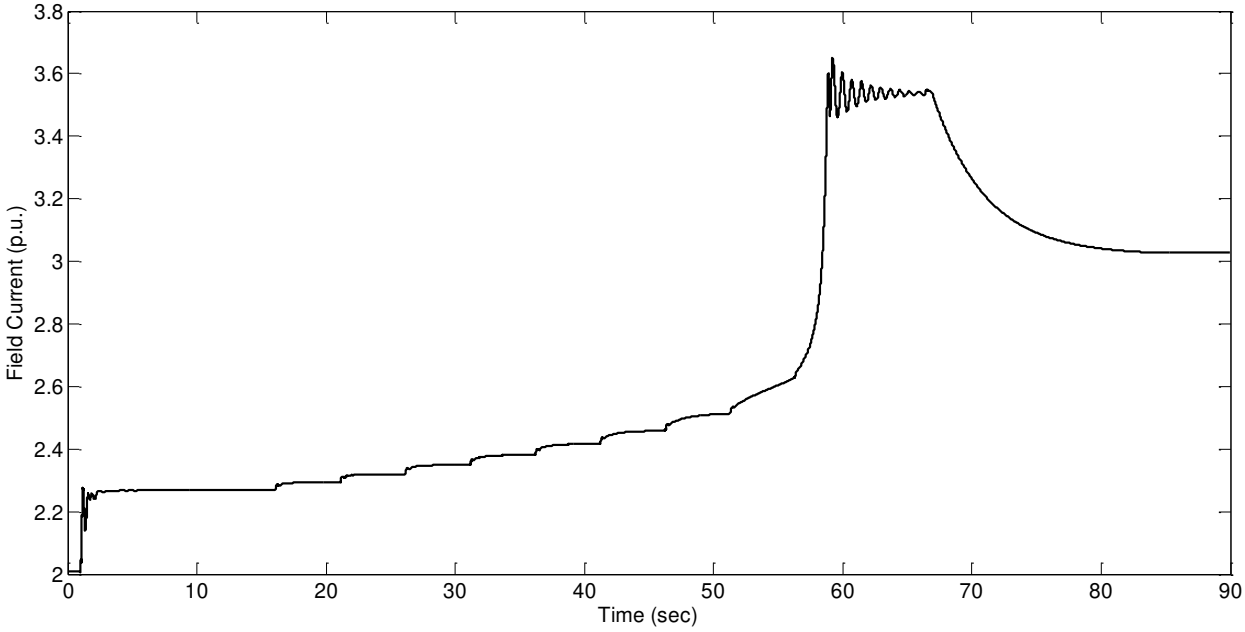

Figure 4.8 Generator G3 Field Current

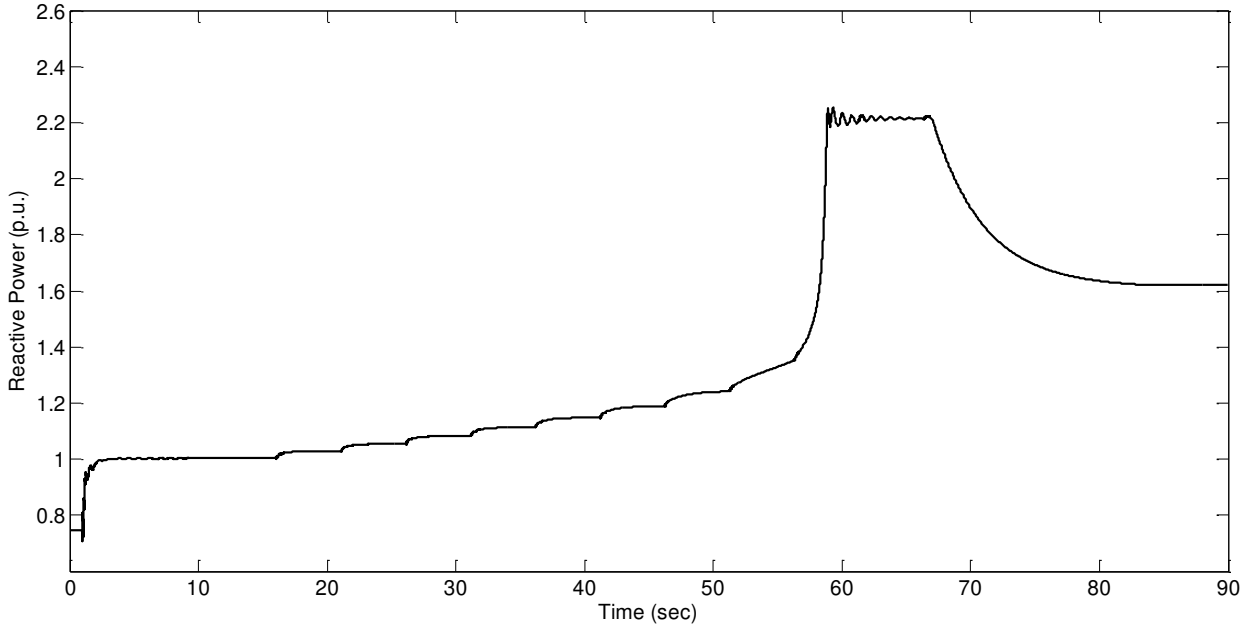

Figure 4.9 Generator G3 Reactive Power Output

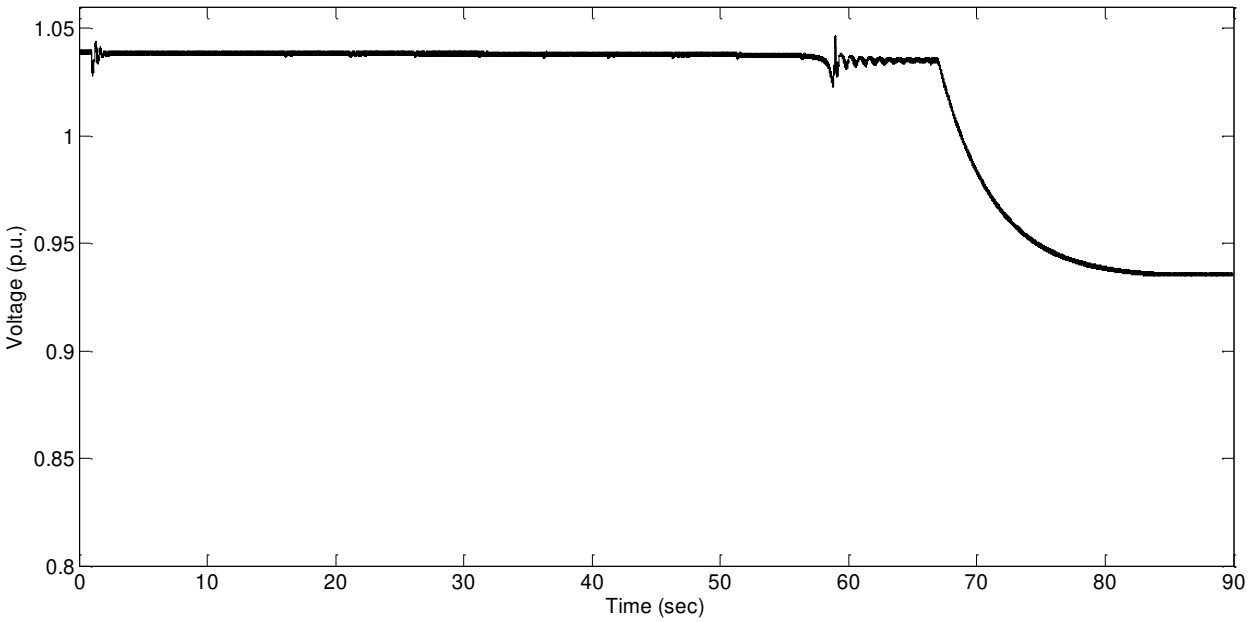

Figure 4.10 Generator G3 Terminal Voltage

4.4 P-index Results

Figures (4.11) and (4.12) show the bus voltage, P-index, and L-index for both load buses 8 and 11. Before the line is lost, the P-index of bus 8 was equal to 0.47 which indicates that the system was already heavily stressed. After the line is lost the P-index increased to 0.58 and continued increasing until it reached a value of 1 at the system point of collapse. On the other hand the L-index had a value of 0.42 before the line was lost and its value changed to 0.49 after the line was tripped out.

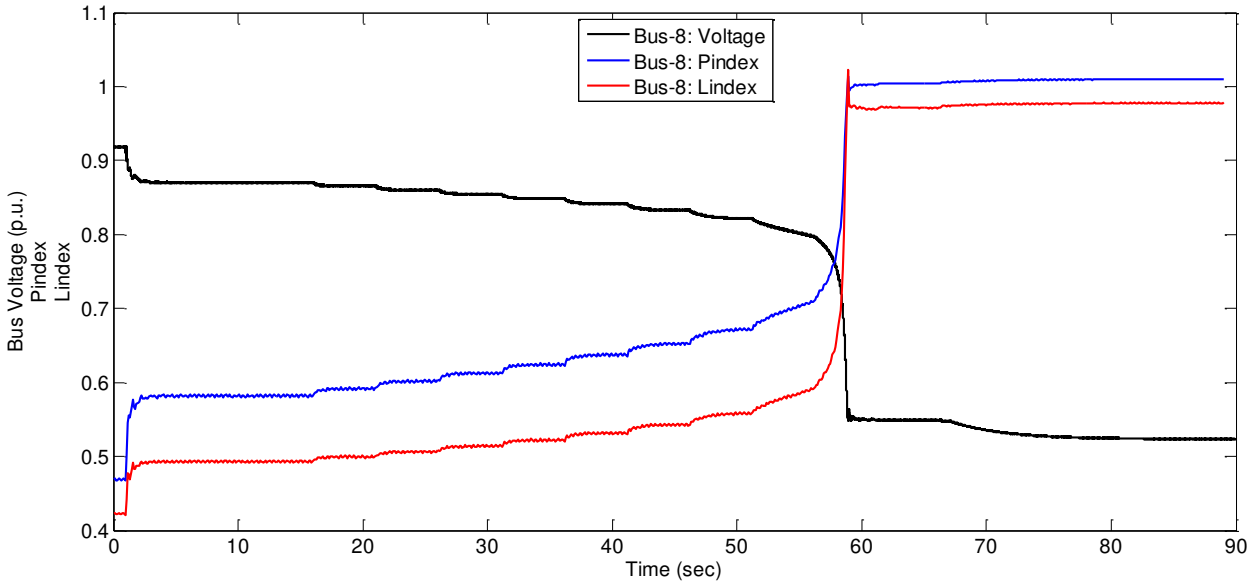

Figure 4.11 Bus-8: Voltage, P-index and L-index

For bus 11, the P-index had a value of 0.5 before the line was lost and its value changed to 0.6 after the line was tripped out. The P-index continued increasing until it reached 1 at the point of collapse. However, the L-index reached a value below 0.85 at the point of collapse.

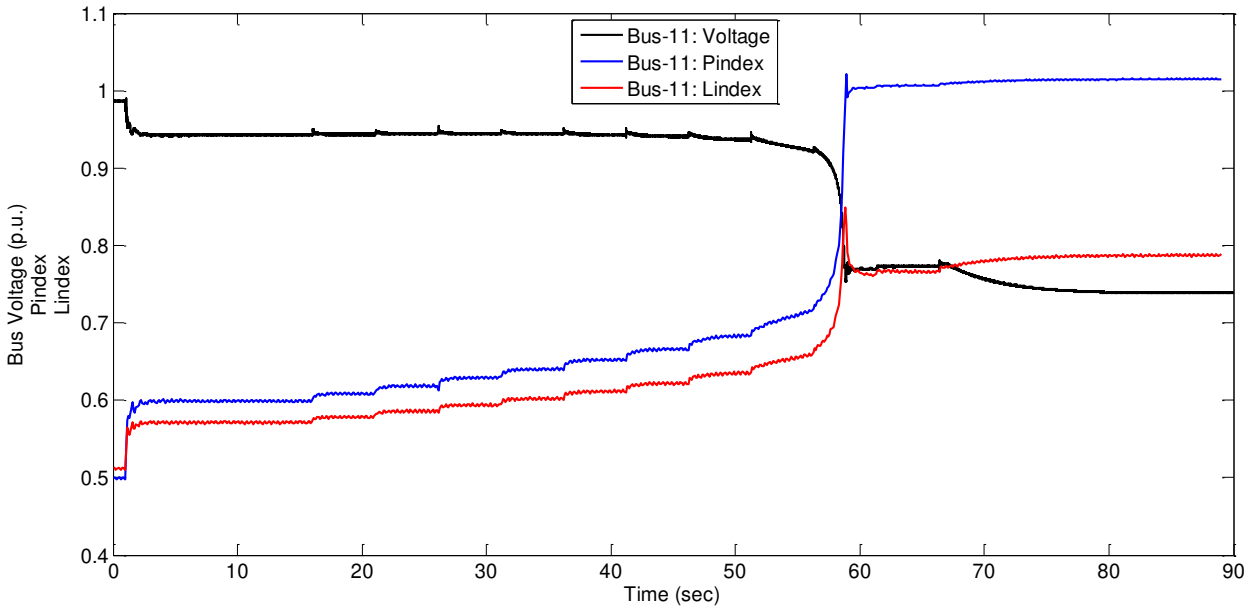

Figure 4.12 Bus-11: Voltage, P-index and L-index

Both the P- and L-indices indicated that bus 11 is the weakest bus. According to the plots shown in Figure (4.13), the P-index indicated that bus 11 is slightly worse than bus 8 whereas the L-index gave a proportionally higher indication of the worst bus. However, even though the L-index indicated that bus 11 is worse; at the point of collapse the L-index had a value of only 0.85 for bus 11 compared to a value of 1 for bus 8.

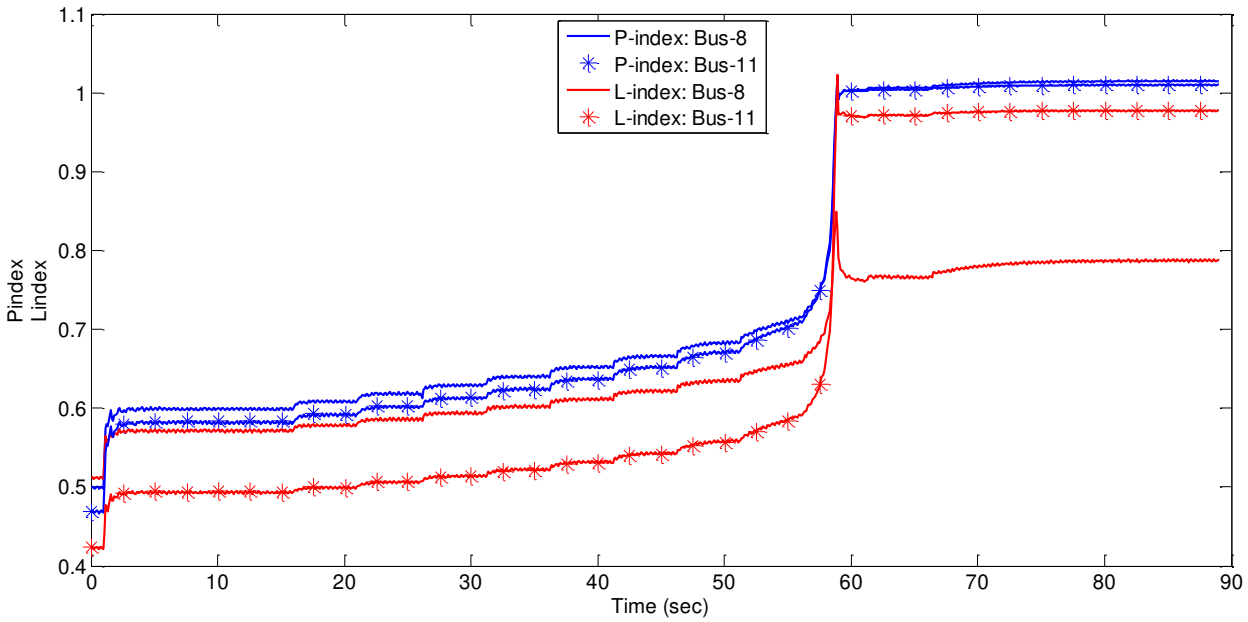

Figure 4.13 P-index and L-index for Both Bus-8 and Bus-11

4.5 Topology Modification Results

The system is initially represented with its last known topology. The line loss is detected through power injection mismatch at buses 6 and 7 and the original system topology is modified accordingly. The P-index is then calculated using the modified system topology. For verification purposes, the P-index is calculated again using the actual system topology, i.e. without the transmission line. As can be seen from Figure (4.14); both methods result in the same values for the P-index.

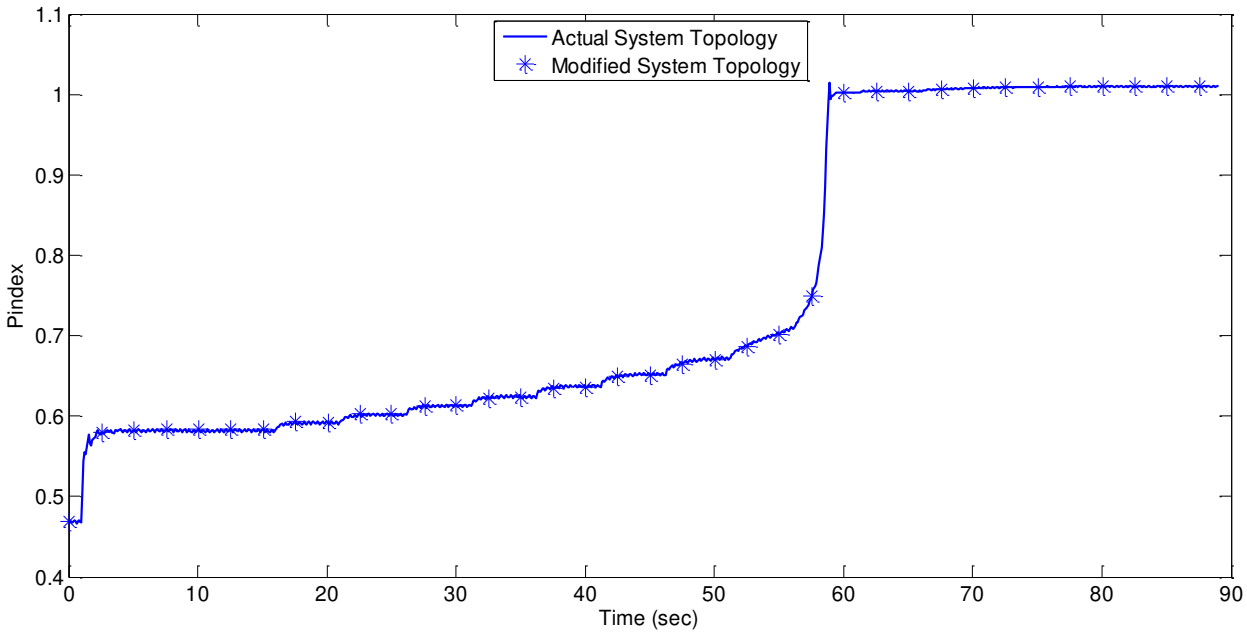

Figure 4.14 P-index using Actual and Modified Topology

4.6 Load Shedding Results

Since the P-index of both buses 8 and 11 exceeded the 0.5 threshold, automatic voltage shedding was initiated. A snapshot of the system at time t=20 seconds was used to calculate the amount to be shed. This 20 seconds delay is purely for demonstrative purposes. Actual load shedding should commence after a much smaller waiting period once the P-index exceeded acceptable threshold. The amount of load to shed is determined according to Equations (3.28) and (3.29) where the desired value for bus 11 P-index was set to be equal to 0.45. The percentage of MW load to be shed is found to be 10.7% (from both buses 8 and 11). The load shedding results are shown in Figures (4.15) and (4.16).

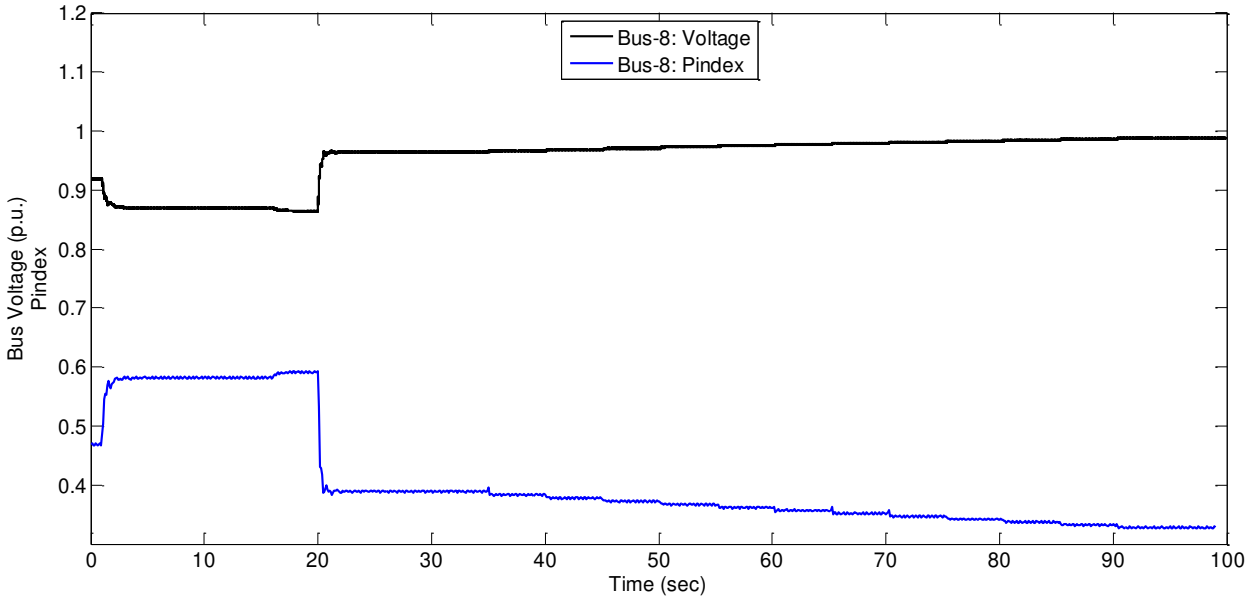

Figure 4.15 Bus-8: Voltage and P-index

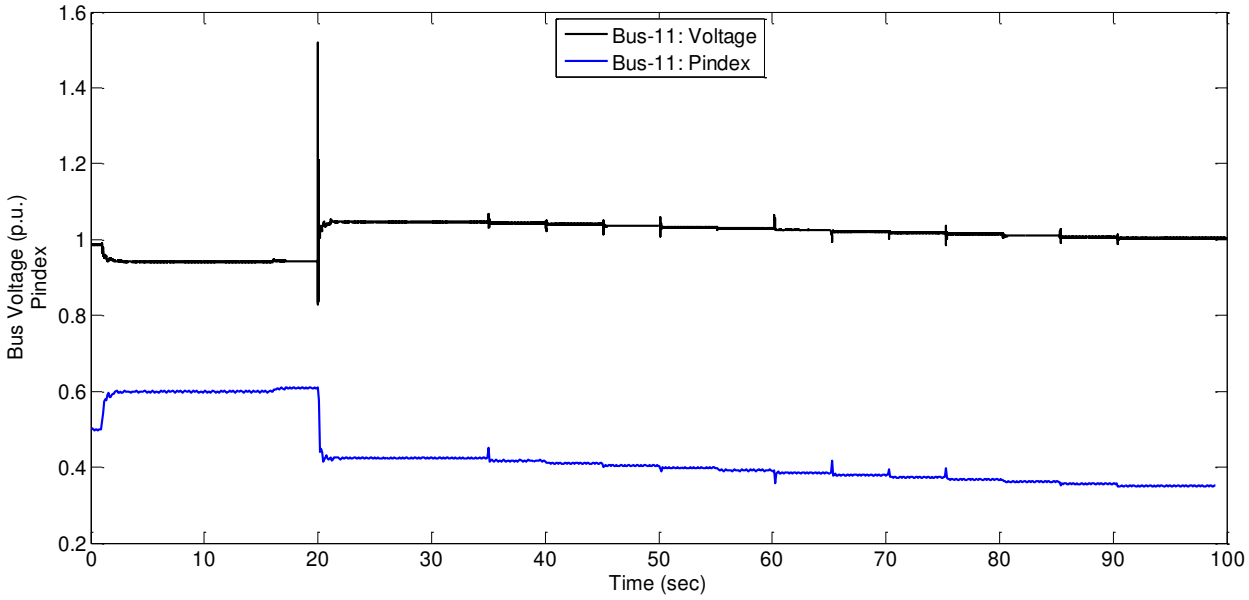

Figure 4.16 Bus-11: Voltage and P-index

The amount of load to be shed is based on the assumption of a constant impedance load model. The constant impedance model has the worst voltage recovery characteristics since the voltage rise would be accompanied by a power increase which would partially offset the intended load reduction. Therefore, as it would be expected, shedding the same amount from a load with different dynamics such as constant power or constant current would result in a better voltage recovery and therefore a better index value. This can be seen from the plots shown in Figures (4.15) and (4.16). For bus 8 where the load is a constant power one, the value of the P-index changed to 0.39 whereas for bus 11 where the load is 50% constant current and 50% constant impedance the P-index changed to a value of 0.42.

CHAPTER 5

CONCLUSION AND FUTURE WORK

5.1 Conclusion

In this work a new voltage stability indicator, the P-index, was proposed. Its value varies from 0 at no load to 1 at the system point of collapse and this holds true for simplified as well as complex systems. This index is based on normalized voltage and power sensitivities and therefore, it conveys a better estimate of absolute stability in comparison to other indices. Furthermore, the proposed index is intuitive and easy to explain in physical terms.

The performance of the P-index was first investigated on the IEEE 14- and 57- bus test systems and compared with another stability indicator: the L-index. The P-index showed a consistent behavior where it always reached a value of 1.0 at the stability limit. However, the same was not true for the L-index. For the 14-bus system the L-index failed to reach its presumed theoretical limit of 1.0 while for the 57-bus system, its value exceeded this limit of 1.0.

The P-index can be used to estimate the system stability margin. This margin is calculated with the assumption that both the system generation and load will move in the same proportion, i.e. the system operating point will change along the same V-P curve.

The P-index can be used for load shedding purposes. However, the P-index is defined based on the same concept of continuation V-P curves. Therefore, if the P-index is to be used as defined then shedding should be performed at all buses in proportion to their loading. Nevertheless, the P-index can

be defined differently with the intention that only the load at one bus will change. The amount of load to be shed is easily estimated in terms of the calculated and desired P-indices.

The calculation of the P-index is simple. It requires the network model and only one snapshot of the system states (voltage magnitudes and angles) and nodal power. The only elaborate calculation required is the inversion of the system Jacobian matrix, which can easily be accomplished in a fraction of a second. This makes the P-index well suited for on-line voltage stability assessment applications.

In the event of a topology change, the system model needs to be modified. In this work, a simple and quick method for recognizing system topological changes was proposed. The method relies on state information and nodal power measurements only, without need to communicate breaker or switch status or transformer tap position. .

The performance of the proposed P-index and load shedding scheme were tested using dynamic simulation on the well known Kundur 10-bus system. The voltage collapse of the system was simulated using Hypersim, a real-time simulation software. The results show that the P-index was perfectly able to assess the system stability conditions and estimate the amount of load that needs to be shed.

5.2 Future Work

The first area of recommended research is the on-line topology processing method using detected nodal injections. This method needs further investigations, particularly on the boundaries of reduced networks. Since it is impossible to use the injections to determine the actual topological changes for the reduced network, a solution could be to perform the opposite; to carry out an exhaustive search of possible topological outages. The outage which results in the minimum error in states and observed injections is then adopted. Processing the exhaustive search is not likely to be time consuming since the network to be searched is a minimal subset of the original network.

The second area of recommended research is the possibility of using the proposed index in conjunction with adaptive under frequency load shedding schemes (UFLS). Several UFLS schemes use voltage related criteria in order to determine the location where shedding would be most effective. In [21] the bus/buses which experience more voltage drop after the disturbance are selected for shedding. Another example is in [22] where the authors use the V-Q margins as an indication of bus voltage behavior and perform shedding from the most voltage sensitive buses. The P-index can be used as a criterion for UFLS since it estimates the absolute voltage-power trend for each load bus thereby, identifying the buses which would be most suited for load shedding.

REFERENCES

[1] Kundur, P., et al., *Definition and classification of power system stability IEEE/CIGRE joint task force on stability terms and definitions.* Power Systems, IEEE Transactions on, 2004. **19**(3): p. 1387-1401.

[2] Gao, B., G. Morison, and P. Kundur, *Voltage stability evaluation using modal analysis.* Power Systems, IEEE Transactions on, 1992. **7**(4): p. 1529-1542.

[3] Löf, P., et al., *Fast calculation of a voltage stability index.* Power Systems, IEEE Transactions on, 1992. **7**(1): p. 54-64.

[4] Berizzi, A., et al., *First and second order methods for voltage collapse assessment and security enhancement.* Power Systems, IEEE Transactions on, 1998. **13**(2): p. 543-551.

[5] De Souza, A.C., C.A. Canizares, and V.H. Quintana, *New techniques to speed up voltage collapse computations using tangent vectors.* Power Systems, IEEE Transactions on, 1997. **12**(3): p. 1380-1387.

[6] Vu, K., et al., *Use of local measurements to estimate voltage-stability margin.* Power Systems, IEEE Transactions on, 1999. **14**(3): p. 1029-1035.

[7] Julian, D., et al. *Quantifying proximity to voltage collapse using the voltage instability predictor (VIP)*. in *Power Engineering Society Summer Meeting, 2000. IEEE*. 2000. IEEE.

[8] Moghavvemi, M. and O. Faruque. *Real-time contingency evaluation and ranking technique*. in *Generation, Transmission and Distribution, IEE Proceedings*-. 1998. IET.

[9] Grijalva, S. and P.W. Sauer, *A necessary condition for power flow Jacobian singularity based on branch complex flows.* Circuits and Systems I: Regular Papers, IEEE Transactions on, 2005. **52**(7): p. 1406-1413.

[10] Verbič, G. and F. Gubina. *A novel concept for voltage collapse protection based on local phasors*. in *Transmission and Distribution Conference and Exhibition 2002: Asia Pacific. IEEE/PES*. 2002. IEEE.

[11] Zhao, J., Y. Yang, and Z. Gao, *A review on on-line voltage stability monitoring indices and methods based on local phasor measurement.* Dianli Xitong Zidonghua(Automation of Electric Power Systems), 2010. **34**(20): p. 1-6.

[12] Kessel, P. and H. Glavitsch, *Estimating the voltage stability of a power system.* Power Delivery, IEEE Transactions on, 1986. **1**(3): p. 346-354.

[13] VERAYIAH, R., et al., *Under Voltage Load Shedding Scheme Using Meta-heuristic Optimization Methods.* Przegląd Elektrotechniczny, 2014. **90**(11): p. 162--168.

[14] *Power Systems Test Case Archive*. Available from: https://www.ee.washington.edu/research/pstca/.

[15] Acharya, N.V. and P. Rao. *A new voltage stability index based on the tangent vector of the power flow jacobian*. in *Innovative Smart Grid Technologies-Asia (ISGT Asia), 2013 IEEE*. 2013. IEEE.

[16] Farrokhabadi, M., *Automated topology processing for conventional, phasor-assisted and phasor-only state estimators*. 2012, Master's thesis, Royal Institute of Technology (KTH).

[17] Farrokhabadi, M. and L. Vanfretti. *Phasor-assisted automated topology processing for state estimators*. in *Electrical Power & Energy Conference (EPEC), 2013 IEEE*. 2013. IEEE.

[18] Qian, C., Z. Wang, and J. Zhang. *A New Algorithm of Topology Analysis Based on PMU Information*. in *Critical Infrastructure (CRIS), 2010 5th International Conference on*. 2010. IEEE.

[19] Wood, A.J., B.F. Wollenberg, and G.B. Sheblé, *Power Generation, Operation and Control*. 2013: Wiley.

[20] Kundur, P., N.J. Balu, and M.G. Lauby, *Power System Stability and Control*. 1994: McGraw-Hill Education.

[21] Abdelwahid, S., et al., *Hardware implementation of an automatic adaptive centralized underfrequency load shedding scheme.* Power Delivery, IEEE Transactions on, 2014. **29**(6): p. 2664-2673.

[22] Seyedi, H. and M. Sanaye-Pasand, *New centralised adaptive load-shedding algorithms to mitigate power system blackouts.* Generation, Transmission & Distribution, IET, 2009. **3**(1): p. 99-114.

APPENDIX A

KUNDUR 10-BUS SYSTEM DATA

The following tables provide the Kundur 10-bus system data as used in this work. Generator G1 is modeled as an Infinite bus. Table 1 provides the machine parameters for both generators G2 and G3. The machine time constants are shown in Table 2. Table 3 provides the transmission lines data. Table 4 provides the transformers data. Generation is provided in Table 5. The Shunt capacitors' reactive power (at nominal voltage) is shown in Table 6. The Load active and reactive power values (at nominal voltage) are presented in Table 7. Finally, the induction motor parameters are shown in Table 8.

Table 1 Machines' Parameters (in p.u. Based on Respective Machine Ratings)

Generator	**MVA Rating**	**Voltage**	R_a	X_d	X_q	X'_d	X'_q	X''_d	X''_q	X_l
G1	2200	13.8 kV	0.0029	1.200	0.700	0.315	0.650	0.200	0.220	0.150
G2	1400	13.8 kV	0.0029	1.200	0.700	0.315	0.650	0.200	0.220	0.150

Table 2 Machines' Time Constants

Generator	T'_{d0}	T'_{q0}	T''_{d0}	T''_{q0}
G1	8	8	0.070	0.065
G2	8	8	0.070	0.065

Table 3 Transmission Lines Data (in p.u. Based on 100 MVA)

Line	R	X	Y
5-6	0.0000	0.0040	0.0000
6-7	0.0015	0.0288	1.1730
9-10	0.0010	0.0030	0.0000

Table 4 Transformers Data (in p.u. Based on 100 MVA)

Transformer	MVA	V	R	X	Ratio
T1	7500	500/13.8 kV	0	0.0020	0.8857
T2	2200	500/13.8 kV	0	0.0045	0.8857
T3	1400	500/13.8 kV	0	0.0125	0.9024
T4	5000	500/13.8 kV	0	0.0030	1.0664
T5	5000	500/115 kV	0	0.0026	1.0200
T6	5000	500/13.8 kV	0	0.0010	--

Table 5 Generation

Generator	P(MW)	V(pu)
G1	3590	0.9800
G2	1736	0.9646
G3	1154	1.0400

Table 6 Shunt Capacitors

Bus	MVAr
7	763
8	600
9	1710

Table 7 Loads

Bus	P(MW)	Q(MVAr)
8	3115	--
11	3420	970

Table 8 Induction Motor Parameters (in p.u. Based on Motor Ratings: 3600 MVA, 13.8 kV)

R_s	0.01
X_s	0.145
R_r	0.008
X_r	0.145
X_m	3.3
H	0.6 Seconds

VITA

Mariana Kamel was born in Khartoum, Sudan in 1990. She received her B.sc – Bachelor of Science in electrical engineering from the University of Khartoum, Sudan, in 2012. From 2012 to 2013, she was employed as a power system analyst by ELECON, an electrical services company in Khartoum, Sudan. In 2014 she started her M.sc – Master of Science in electrical engineering at the University of Tennessee at Chattanooga. She was awarded her master's degree in August 2016. Her interests in power system include power system analysis, power system stability and control.